Characterizing Rider Safety in terms of Asphalt Pavement Surface Texture

CFIRE 07-08
October 2013

National Center for Freight & Infrastructure Research & Education
Department of Civil and Environmental Engineering
College of Engineering
University of Wisconsin–Madison

Authors:
Hussain U. Bahia,
Mozhdeh Rajaei,
Nima Roohi Sefidmazgi

Principal Investigator:
Hussain U. Bahia, Ph.D.,
Professor
Department of Civil & Environmental Engineering
UW-Madison

i

Technical Report Documentation Page

1. Report No. 07-08	2. Government Accession No.	3. Recipient's Catalog No. **CFDA 20.701**
4. Title and Subtitle **Characterizing Rider Safety in terms of Asphalt Pavement Surface Texture**		5. Report Date October 2013
		6. Performing Organization Code
7. Author/s **Hussain Bahia, Mozhdeh Rajaei, Nima Roohi Sefidmazgi**		8. Performing Organization Report No.
9. Performing Organization Name and Address National Center for Freight and Infrastructure Research and Education (CFIRE) University of Wisconsin-Madison 1415 Engineering Drive, 2205 EH Madison, WI 53706		10. Work Unit No. (TRAIS)
		11. Contract or Grant No. **DTRT06-G-0020**
12. Sponsoring Organization Name and Address Research and Innovative Technology Administration U.S. Department of Transportation 1200 New Jersey Ave, SE Washington, D.C. 20590		13. Type of Report and Period Covered **Final Report [12/01/12 - 09/30/13]**
		14. Sponsoring Agency Code
15. Supplementary Notes **Project completed for USDOT's RITA by CFIRE.**		

16. Abstract

The overall goal of the pavement design is to meet the intended service life and more importantly to provide a safe riding surface for the traveling public. Therefore, pavements can experience structural failure (i.e. rutting or cracking) or functional failures, where the pavement becomes unsafe from a riders perspective due to a lack of sufficient surface texture (friction). Several countries within the European Union have specifications related to measurement of surface texture already in place to ensure a minimum level of friction. The barrier to implementing similar practices in the United States is in further development of friction measurement and analysis methods. Measuring pavement friction involves specialized equipment with a relatively high initial cost. In addition, many devices require that measurements be made on field pavement sections, incurring further delay in opening a new pavement to traffic. Several recent studies have correlated asphalt pavement surface texture with friction using relatively inexpensive, non-intrusive devices. These devices can be used in the laboratory as well as in the field and have shown promise in estimating not only pavement surface texture and friction, but also noise emissions. With further development, these methods will give pavement designers the necessary tools to evaluate asphalt pavement surface texture in terms of pavement friction, promoting development of new specifications. This project refines and applies these methods to several plant produced mixtures to estimate surface texture and friction. Limits on the mix design parameters most affecting rider safety (friction) will be proposed.

17. Key Words Friction, Pavement surface texture, Mean Profile Depth	18. Distribution Statement No restrictions. This report is available through the Transportation Research Information Services of the National Transportation Library.		
19. Security Classification (of this report) Unclassified	20. Security Classification (of this page) Unclassified	21. No. Of Pages 56	22. Price **-0-**

Form DOT F 1700.7 (8-72)   **Reproduction of form and completed page is authorized.**

DISCLAIMER

PROJECT DECRIPTION

The overall goal of the pavement design is to meet the intended service life and more importantly to provide a safe riding surface for the traveling public. Therefore, pavements can experience structural failure (i.e. rutting or cracking) or functional failures, where the pavement becomes unsafe from a riders perspective due to a lack of sufficient surface texture (friction). Several countries within the European Union have specifications related to measurement of surface texture already in place to ensure a minimum level of friction. The barrier to implementing similar practices in the United States is in further development of friction measurement and analysis methods. Measuring pavement friction involves specialized equipment with a relatively high initial cost. In addition, many devices require that measurements be made on field pavement sections, incurring further delay in opening a new pavement to traffic. Several recent studies have correlated asphalt pavement surface texture with friction using relatively inexpensive, non-intrusive devices. These devices can be used in the laboratory as well as in the field and have shown promise in estimating not only pavement surface texture and friction, but also noise emissions. With further development, these methods will give pavement designers the necessary tools to evaluate asphalt pavement surface texture in terms of pavement friction, promoting development of new specifications. This project refines and applies these methods to several plant produced mixtures to estimate surface texture and friction. Limits on the mix design parameters most affecting rider safety (friction) will be proposed.

TABLE OF CONTENTS

LIST OF FIGURES

LIST OF TABLES

CHAPTER 1. INTRODUCTION

SIGNIFICANCE AND PURPOSE

In recent years, pavement designers are increasingly challenged by achieving ideal surface friction properties to enhance drivers' safety, through mixture design and material selection. Sufficient pavement texture is needed to ensure adequate friction between tires and the pavement, though too much texture can result in detrimental consequences related to tire wear and fuel consumption. Only with sophisticated finite element modeling software and analysis tools have researchers begun to understand how complex the interaction at the tire-pavement interface truly is. Yet characterization of the tire surface alone is insufficient for describing the tire-pavement interaction, as pavement surface texture characteristics also contribute significantly to the tire-pavement relationship. Pavement mixture design specifications and material selection influences skid resistance, therefore, a clear understanding of relationship between pavement mixture design properties and surface friction is needed.

In the present study, the "Surface Laser Profilometer" (SLP) device is used to measure surface texture, by scanning the surface of laboratory compacted and field core samples, from which a surface texture profile is derived. Surface texture data is analyzed to calculate the "Mean Profile Depth" (MPD). After the SLP scans the mixture sample or pavement surface profile, macro-texture (spatial wavelengths ranging from 0.5 mm to 50 mm) parameters and micro-texture (spatial wavelengths less than 0.5 mm) parameters can be extracted using signal processing techniques and related to friction properties.

Statistical analysis and neural networks modeling are used to find relationship between the MPD results estimated from laser profilometer measurements and mixture design properties (i.e., aggregate size, gradation curve shape, binder content, air voids, and volumetric properties). Promising trends are observed in the data that can potentially be used as guidance for mixture designers to optimize mixture design properties in order to achieve better pavement surface friction and thus enhance drivers' safety.

Additionally, relationships between field measured friction (mainly Friction Number (FN)) and laboratory measured texture parameters are developed. FN values measured by using the locked-wheel tire test in the field were taken from the MnROAD test track database and used for analysis. It is shown that there is a correlation between FN and MPD, presenting the opportunity to achieve a target value of friction in the field through materials selection in the mix design phase supplemented with laboratory measurement and analysis of friction properties. Such relationships between laboratory measurements and field friction could lead to better control of pavement surface friction, thus allowing for control of both pavement structural and functional performance.

Using statistical analysis and artificial neural network modeling, mixture design parameters (i.e. volumetric and aggregate gradation properties) could be related to laboratory texture measurements (MPD). Therefore, knowing mixture design properties can lead to the estimation of road texture parameters. It is also shown that pavement texture is mainly controlled by aggregate gradation and mixture volumetric characteristics. Additionally, it was shown that increasing the distance of the gradation curve from the

maximum density line is more important than the overall coarseness or fineness of the gradation in terms of increasing the expected texture. Laboratory measured friction parameters (MPD) can be related to field friction values (FN) using regression analysis. Utilizing the models developed in this study, by further investigation, mixture designers can have a guideline to estimate friction. Models developed in this study showed that the measurements for field and laboratory compacted samples from SLP device can be used to estimate friction parameters.

RESEARCH OBJECTIVES

The objectives of this work are focused on developing methods to estimate field friction based on laboratory measured samples, and understanding how different mixture design parameters affect surface texture characteristics. The specific objectives include:

1. Evaluating the relationship of mixture design parameters (i.e. volumetric and aggregate gradation properties) to laboratory texture measurements (MPD).
2. Estimation of pavement texture parameters based on mixture design properties.
3. Evaluating the relationship of laboratory measured texture parameters (MPD) to field friction values (FN).
4. Proposing a guideline model for mixture design to estimate friction.

CHAPTER 2. LITERATURE REVIEW

This chapter highlights the findings of the investigation in literature, focusing mainly on texture and friction of asphalt pavements. It begins with an introduction to safety considerations, surface texture characterization, and factors influencing surface texture of pavements. The second section focuses on friction characterization, friction mechanisms between tire and pavement, factors influencing friction, and friction measurement methods. The literature review also includes a description of the measurement and analysis system used for this research.

Safety Considerations

The relationship between surface texture and accident rates has been well documented over the past 30 years (Noyce et al 2007, Hall et al 2009). Safety becomes particularly important under wet conditions, where a lack of adequate surface texture dramatically increases the risk of hydroplaning and loss of vehicular control. Thus, a primary functional quality of pavements is to provide adequate friction, as it is linked to the safety of the roadway.

Increasing demand for mobility which results in high number of vehicles and more frequent crashes makes the safety of both the road and driversa high priority issue.. alone recent study estimates that the cost for highway accidents in 2000 exceeded $230 billion (Noyce et al 2007). Many of these crashes are tied to wet road conditions, and possibly to inadequate friction characteristics. This cost is expected to increase with increasing demand for transportation facilities domestically and abroad. Therefore, advancing the knowledge regarding improved friction characteristics and adopting better design methods to improve friction could refocus limited financial resources being spent today on crash investigations.

Because surface texture is directly related to friction, and particularly micro-texture (spatial wavelengths less than 0.5 mm) and macro-texture (spatial wavelengths ranging from 0.5 mm to 50 mm) levels, measuring surface texture serves as an indicator for friction, and hence for safety. Macro-texture, and to a lesser degree micro-texture, is a major contributor to friction safety characteristics (Hall et al 2009). High levels of macro-texture allow for water drainage, which minimizes the risk of hydroplaning in wet conditions.

Other studies have investigated the link between wet-weather crashes and pavement friction. Rizenbergs et al found higher wet crash rates for lower values of skid number (Rizenbergs et al 1972). Giles et al and Cairney investigated crash incidence as a function of skid number and demonstrated that crash incidence increases quickly once a minimum threshold value is reached (Giles et al 1962, Cairney 1997). McCullough and Hankins showed that most crashes occur with low pavement friction levels and very few crashes occur with high levels of pavement friction (McCullough and Hankins 1966). Kamel and Gartshore described how resurfacing a few dangerous sections of Canadian highways significantly

3

reduced crashes in wet and dry conditions (Kamel & Gartshore 1982). Wallman and Astrom suggested that increasing pavement friction can significantly reduce the incidence of crash rates (Wallman & Astrom 2001). Kuttesch has suggested that when friction level falls below a minimum threshold value, the likelihood of wet crashes increases significantly (Kuttesch 2004). In summary, many studies have shown that safety is tied to pavement friction, and friction is related to surface texture. Thus, improving surface texture characterization methods and friction measurement methods can lead to fewer crashes and safer roads.

Surface Texture Characterization

Surface texture refers to asperities in the pavement surface that arise from the combination of different aggregate shapes and sizes used in asphalt mixtures. Surface texture is defined in terms of wavelength (λ, distance along the surface) and amplitude (a, height above the surface). Fundamentally, surface texture is a the property that can be controlled in pavement design that affects the friction and safety in roadways. Based on the definition by the Permanent International Association of Road Congresses (PIARC) in 1987, surface texture is divided into four ranges in terms of texture wavelength and amplitude (Henry, 2000). The micro-texture which is the smallest range, represents the wavelengths smaller than 0.5 mm. The macro-texture refers to wavelengths from 0.5 mm to 50 mm. The roughness on the surface of each coarse aggregate is related to micro-texture while the overall pavement surface roughness (i.e. different aggregate arrangement) can be described by macro-texture (Ivan, et al., 2010). The other two ranges of surface texture are called Mega-texture and Unevenness. Mega-texture refers to spatial wavelengths ranging from 50 mm to 0.5 m with amplitudes ranging from 0.1 mm to 50 mm. The largest range is called unevenness or roughness and encompasses spatial wavelengths greater than 0.5 m. Figure 1 displays the different ranges of surface texture graphically, and Table 1 summarizes these ranges. Each range of surface texture impacts tire-pavement behavior differently, so coupling the appropriate spatial scale with the effect in question is critically important.
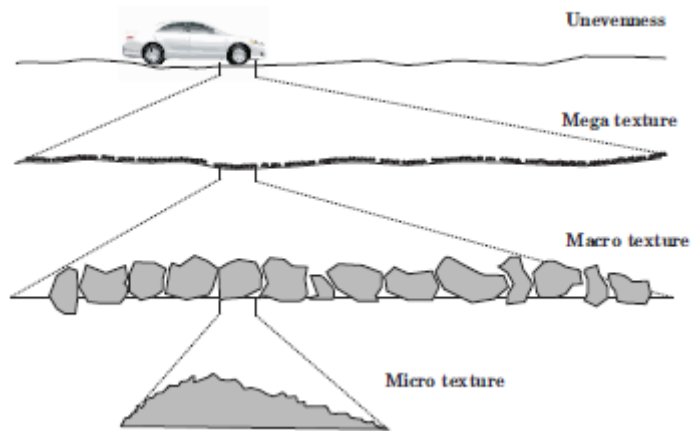
Figure 1. Graphical representations of four surface texture regimes.

Table 1. Texture wavelength ranges

Region	Wavelength
Micro-texture	$\lambda < 0.5$ mm
Macro-texture	0.5 mm $< \lambda <$ 50 mm
Mega-texture	50 mm $< \lambda <$ 500 mm
Unevenness	0.5 m $< \lambda <$ 50 m

The influence surface texture at different spatial scales on vehicle impacts is provided in Figure 2. At large texture wavelengths ($\lambda > 50$ mm) and low spatial frequencies ($f < 20$ Hz), detrimental effects are observed in terms of rider comfort, vehicle wear, vehicular noise, rolling resistance, and tire-road friction. In the mega-texture regime, rolling resistance and vehicle noise become particularly significant. As the spatial frequency increases to the macro-texture range, tire-road friction becomes more significant. Thus, optimizing the surface texture requires a balance of sufficient friction, and minimal adverse vehicle impacts and costs.

Texture Wavelength

| 0.00001 | 0.0001 | 0.001 | 0.01 | 0.1 | 1 | 10 | 100 | ft |
| 10^{-6} | 10^{-5} | 10^{-4} | 10^{-3} | 10^{-2} | 10^{-1} | 10^{0} | 10^{1} | m |

Micro-texture — Macro-texture — Mega-texture — Roughness/Unevenness

Friction

Ext. Noise

Int. Noise

Splash/Spray

Rolling Resistance

Tire Wear

Tire/Vehicle Damage
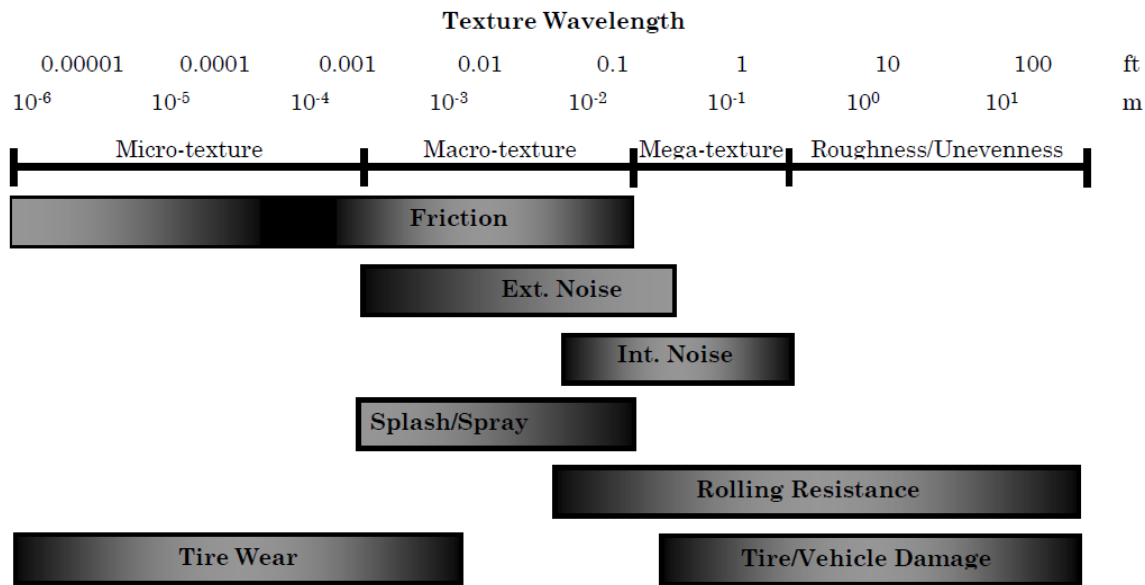
Note: Darker shading indicates more favorable effect of texture over this range.

Figure 2. Influence of texture wavelength on vehicle response.

Current methods used to characterize surface texture, mainly rely on the mean profile depth (MPD). MPD provides a a two-dimensional representation of the surface texture (ISO 13473-1 2004). However, this parameter only provides averaged values for surface texture and does not have sufficient resolution to quantify the distribution of asperities at the pavement surface. A schematic of determination of MPD is provided in Figure 3**Error! Reference source not found.** Although the MPD is simple to measure and has shown some relationships to pavement friction, it has been recognized that knowing the distribution of surface asperities leads to improved methods for friction characterization. Spectral analysis techniques are suitable for quantifying the distribution and may improve upon MPD by capturing the texture distribution over a spectral scale encompassing multiple texture regimes. The decomposition of the texture to smaller scales allows for better control of friction properties, based on this concept there is an opportunity include consideration of friction into the mix design process by defining the impacts of aggregate and mixture volumetric properties on mixture surface properties. A simple method for measuring the distribution is not yet available.

Mean Profile Depth (MPD) =
$$\frac{\text{Peak level (1st)} + \text{Peak level (2nd)}}{2} - \text{Average level}$$

Profile Depth (PD)

Mean Profile Depth (MPD)

Peak level (1st)

Peak level (2nd)

Average level

(First half of baseline)

(Second half of baseline)

Baseline

Estimated Texture Depth (ETD)
ETD = 0,2 + 0,8 MPD
(See 7.9)
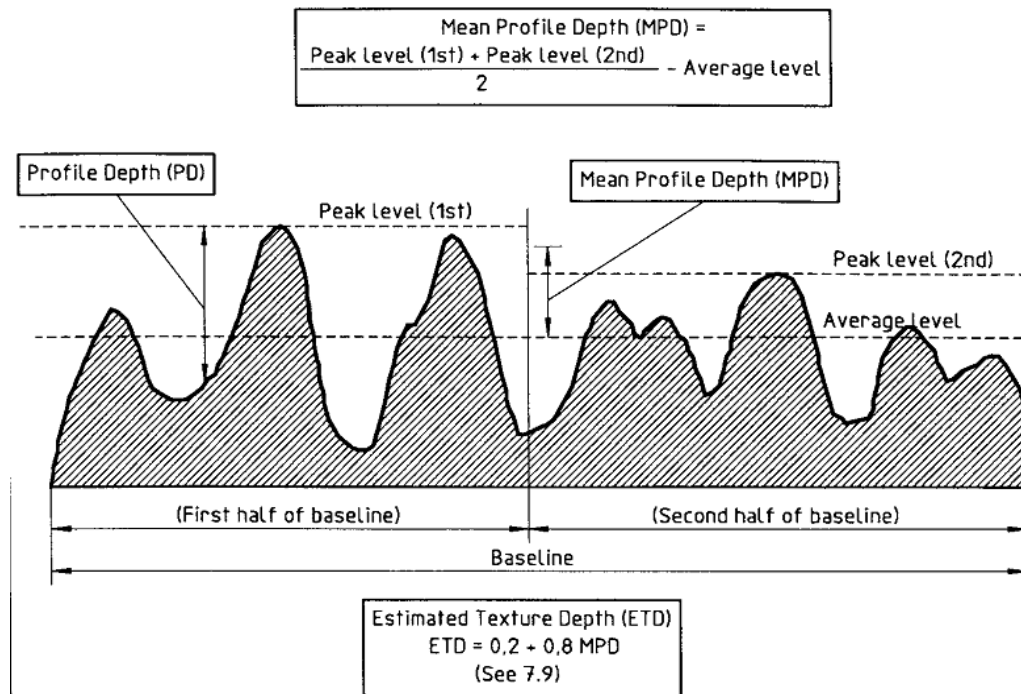
Figure 3. Illustration of mean profile depth.

FRICTION CHARACTERIZATION

Friction is defined as the force that acts opposite to the direction of motion imparted by the pavement surface on a rotating tire. A rolling or sliding tire will generate friction as it moves across the pavement surface. In general, higher levels of friction correspond to greater operator control of the vehicle (Hall et al 2009). The friction coefficient μ represents the quotient of the tangential friction force F and the vertical load F_w imparted from the vehicle to the axle and wheel hub. Figure 4 shows two idealized tire-roadway interaction diagrams and depicts the forces on a rotating tire due to contact with the pavement surface in free-wheeling and constant-braked configurations.
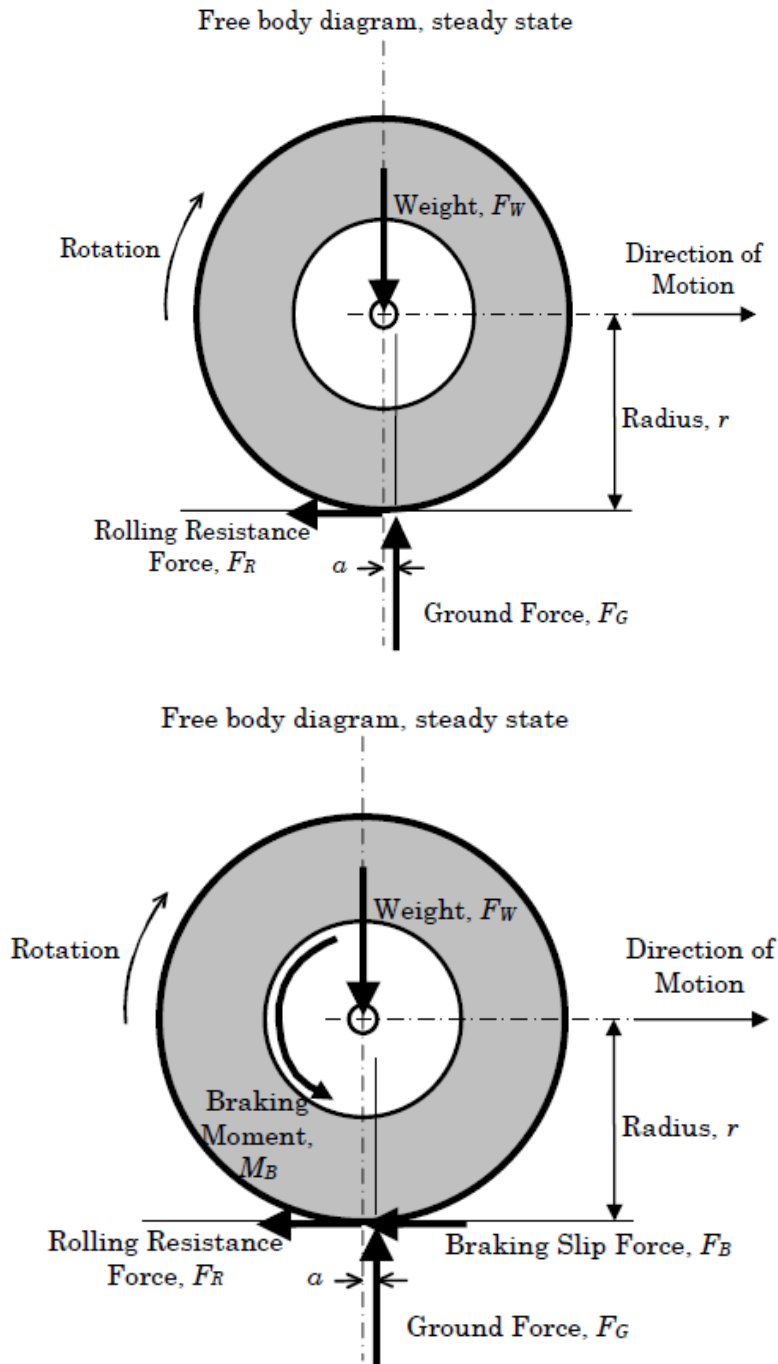
Figure 4. Tire free-body diagrams.

Friction at the tire-pavement interface comprises two friction components in longitudinal and tangential directions. Longitudinal friction forces manifest in the direction of travel in two ways (Hall et al 2009). When the tire is free to roll and no brakes are applied, the relative speed between a point on the tire circumference and the pavement is zero. This is referred to as the slip speed S. With the brakes applied, the slip speed increases from zero to

the speed of the vehicle. Meyer described this relationship mathematically as follows (Meyer 1982):

$$S = V - V_P = V - (0.68 \times \omega \times r) \tag{1}$$

Where:
- S Slip speed, mi/hr.
- V Vehicle speed, mi/hr.
- V_P Average peripheral speed of the tire, mi/hr.
- ω Angular velocity of the tire, radians/sec.
- r Average radius of the tire, ft.

Two conditions are worth noting. With no brakes applied, the average peripheral speed of the tire V_P equals the vehicle speed V. In this case the slip speed S is zero. With brakes fully applied, the peripheral speed of the tire V_P is 0 such that the vehicle speed V equals the slip speed S. Slip speed is important because it will be one of the parameters accounted for in the friction models and indices that will be presented in following sections. Because the slip speed is strongly related to macro-texture, there now exists a means to connect vehicle dynamics with friction characteristics.

Figure 5 depicts the relationship between the friction coefficient and tire slip. In the free-rolling condition, the coefficient of friction approaches zero and increases to a critical peak friction value as the tire slip and braking increases. Beyond the critical slip value, the coefficient of friction diminishes to a terminal value as the fully-locked, full-sliding condition is reached (Hall et al 2009, Henry 2000).
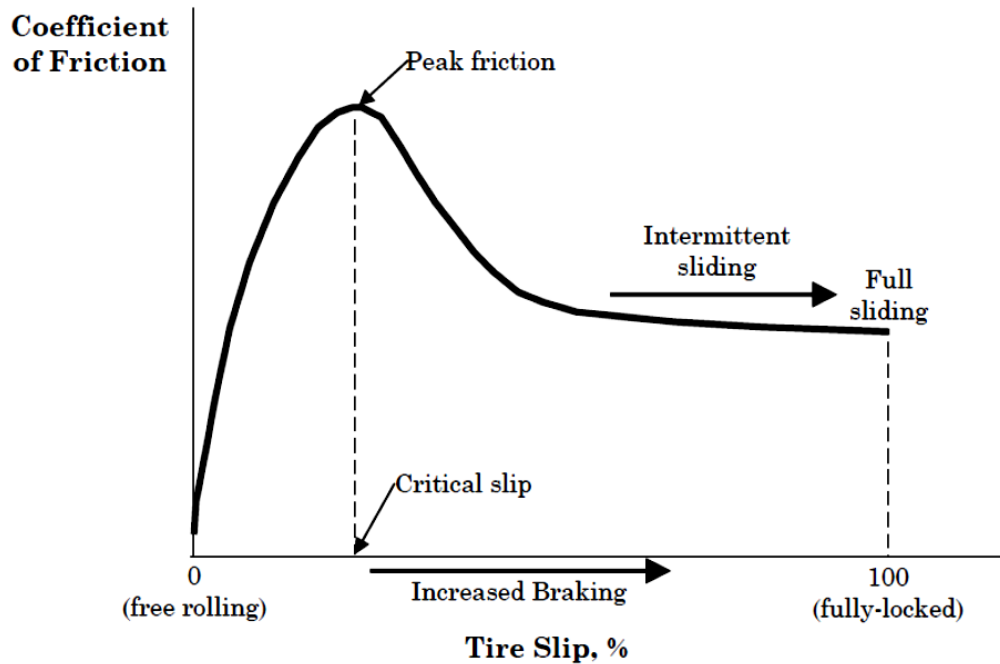
Figure 5. Friction coefficient and tire slip relationship.

A second source of friction originates from lateral friction forces. Lateral friction forces manifest as a vehicle turns, changes lanes, or compensates for cross winds or pavement cross-slopes (Hall et al 2009). The lateral friction force acts outward on tire tread elements and is counter to the centripetal force acting to pull the vehicle inward toward the center of a curve.

Factors Affecting Friction

Factors affecting friction can be divided into four categories which are pavement surface characteristics, vehicle characteristics, tire characteristics, and environmental conditions (Hall, et al., 2009; Rado, 2005). The focus of this study is to characterize the pavement surface characteristics (i.e. surface texture) using newly developed lab tests and analysis and developing relations between important pavement material and design factors with pavement surface texture and friction as result . Based on the literature review performed in this study the factors listed in Table 2 have been found to potentially affect surface friction. Factors mentioned in Table 2 are used to identify and prioritize factors entered into the analysis performed in the present work.

Table 2. Mixture Properties Affecting Surface Texture in Asphalt Pavements (Henry, 2000; Hall, et al., 2009; Sandberg & Ejsmont, 2000; AASHTO, 1976; PIARC, 1995; Ahammed & Tighe, 2009)

Property	Texture Range
Nominal Maximum Aggregate Size (NMAS)	Macro-Texture
Mixture Coarse Aggregate Type (shape)	Macro-Texture Micro-Texture
Mixture Fine Aggregate Type (shape)	Macro-Texture Micro-Texture
Asphalt Binder Content	Macro-Texture
Aggregate Gradation	Macro-Texture
Mixture Air Voids	Macro-Texture

As shown in the Table 2, aggregate shape and texture are more important to control micro-texture while gradation, mixture properties and compaction are mainly affecting macro-texture.

A significant amount of research has focused on tire and vehicle characteristics, with tire companies investing considerable resources in the interest of designing durable tires with efficient tread patterns. Vehicle and tire considerations are not the focus of this study, as this type of analysis necessitates use of finite element models to capture vehicle dynamics and is beyond the scope of this investigation. Rather, the focus here will be on how pavement surface characteristics affect friction and how to control pavement surface texture using current mix design procedures.

Properties of materials used in pavements typically affect micro-texture and macro-texture, while construction techniques and pavement distresses typically affect larger texture wavelength regimes such as mega-texture and unevenness. If particular mix design parameters exhibit a significant effect on micro-texture and macro-texture properties, then the mix design can be controlled to achieve optimal levels of micro-texture and macro-texture wavelengths as these regimes affect noise and friction.

Friction number (FN)

The friction number (FN) or skid number (SN) is the average coefficient of friction measured by a locked-wheel test device as specified in ASTM E274. Almost all states in the United States are using locked-wheel devices to evaluate friction. This method tests frictional properties for emergency braking without anti-lock braking systems. The method differs from side-force or fixed-slip methods in that the slip speed is equal to the vehicle speed, the wheel remains locked, and there is no rotation of the tire (Hall, et al., 2009). Tests can be conducted with ribbed tire or smooth tire at a range of speeds. The friction number (FN) is calculated as:

$$FN \ (V) = 100 \ \mu = 100 \ \times \frac{F}{W} \tag{2}$$

Where: V Velocity of the test tire, km/hr.
                          μ Coefficient of friction.
                          F Tractive horizontal force applied to the tire, kg.
                          W Vertical load applied to the tire, kg.

Friction Measurement Methods

Friction measuring devices may be classified as devices operating at highway speeds and devices requiring traffic control (Hall, et al., 2009). Highway-speed friction test methods encompass locked wheel (ASTM E274), side-force (ASTM E670), fixed-slip (various ASTM standards) and variable-slip (ASTM E1859) test devices. Each of these devices utilizes a tow trailer or specially-instrumented vehicle. The test methods report various measurement indices, such as friction number (FN). The devices can be used for network-level friction monitoring and field testing, though some devices are limited in their ability to measure curved sections and heavily damaged sections. The advantage of these devices is that they utilize full-scale tires at highway speeds, which gives a more accurate representation of friction performance of actual vehicle tires. Major disadvantages include the level of technical training required, cost, and sensitivity to surface irregularities such as potholes and cracks.

Rather than using highway-speed devices, this study makes use of devices requiring traffic control. While stopping distance measurements (ASTM E445) and deceleration rate measurements (ASTM E2101) are typically used for crash investigations, other examples of test methods requiring traffic control are more applicable to this investigation. One portable tester used to measure friction characteristics is the Dynamic Friction Tester (DFTester). Portable devices used to evaluate surface texture are the circular track meter (CTM), and a stationary linear profiler (SLP).

Test Methods

This study focuses on the results of three macro-texture characterization methods which is a volumetric method, and two laser methods, one of which is circular while the other is linear. For macro-texture (0.5 mm < λ < 50 mm) evaluation, the Circular Track Meter (CTM) provides estimates of high-speed friction potential. The next device, the Stationary Linear Profiler (SLP), has been modified and used extensively in this study, as will be described in detail. It was selected as the most promising method to use to evaluate both macro-texture and micro-texture in both the laboratory and field.

Circular Track Meter (CTM)

The Circular Track Meter (CTM) is a non-contact laser device used to analyze pavement macro-texture. ASTM offers specifications for usage of the device (ASTM E2157 2009). Manufactured in Japan by the Sunny Koken Company, the charge-coupled device (CCD) laser profiler is mounted on a rotating arm at a fixed location above the surface. A laptop computer controls the device operation. After initiating a measurement, a direct current (DC) motor drives the arm and traces a circle with a diameter of 284 mm on the pavement surface. Once the measurement is complete, software algorithms partition the segment into eight sections. Mean profile depth (MPD) and root mean square (RMS) values are computed for each section. The CTM reports 1024 points, a convenient number of points for applying Discrete-Time Fourier Transform (DFT) methods to determine the texture spectrum. Figure 6 shows the device. Applied Pavement Technologies, Inc. provided the CTM equipment to researchers for evaluation.

Figure 6. The Circular Track Meter (CTM) is used to evaluate pavement macro-texture.

The CTM delivers a precise estimate of pavement macro-texture indicators, including mean profile depth (MPD) and root mean square (RMS) values. The precision value for eight measurements on same surface is 0.03 mm (ASTM E2157 2009). The device also collects a sufficient number of data points for spectral analysis, which will be explained in subsequent sections. Furthermore, it is a non-destructive test method and thus can be used for evaluation of in-service pavements. .

Despite all advantages, the CTM also has a few disadvantages. The cost of the CTM may prohibit laboratories or state highway agencies from investing in this device. More training is needed to operate this device compared to other devices. Due to the static nature of the device, traffic control is required for field evaluations. The device also requires samples with a minimum physical size of 600 mm by 600 mm. The required sample size limits laboratory evaluations to those labs with access to slab compaction or similar devices.

Many researchers have experimented with the CTM device. Flintsch et al compare macro-texture measurements of three laser devices and the sand patch method (Flintsch, et al., 2003). The experimental design encompassed the Virginia Smart Road, in-service highways, and airfield surfaces. Of the three laser devices evaluated, the CTM demonstrated the highest correlation to volumetric macro-texture measurements. Hanson and Prowell compare CTM MPD measurements with Sand Patch Method (SPM) MTD measurements at the NCAT Test Track for a variety of pavement surfaces (Hanson & Prowell, 2004). Results indicate strong relationships between CTM and SPM values. Perhaps surprisingly, the study found that CTM measurements are more variable than SPM results and suggests that less technician skill is required to operate the CTM compared to other macro-texture measurement devices.

Stationary linear profiler (SLP)

Improved surface characterization technologies utilizing simple laser-based profiling techniques are effective for quantifying texture properties (Losa et al 2005, Losa et al 2007, Losa & Leandri 2010). Linear profiling methods have been used on pavement surfaces for the past 50 years. Use of profiling methods, and particularly methods that can be used at highway speeds, have grown in recent years as highway agencies have recognized the need for improving pavement management strategies and assessing both structural and functional distresses. Profilers have been used extensively to measure surface roughness. More recently, linear profiling methods have been used to estimate frictional properties. As an extension of these concepts, signal processing theories it is possible to define two-dimensional texture profiles to evaluate the texture spectrum.

Laser profilers are differentiated as mobile profilers and stationary profilers in International Organization for Standardization (ISO) standards. Mobile profilers are non-contact devices attached to vehicles that are used to measure pavement surface profiles at highway speeds. Stationary profilers are also non-contact devices but they can be used in field and laboratory environments while remaining static. A stationary linear profiler (SLP) is the primary device used here to evaluate macro-texture and for comparison to other macro-texture and micro-texture measurement methods. Specifications for both mobile and stationary laser profilers are outlined in a series of ISO standards (ISO 13473 2002/2004/2008). ASTM standards provide less direction, though methods are given for calculating mean profile depth (ASTM E1845 2009).

The SLP assembly used in this study, shown in Figure 7, was developed as part of the Asphalt Research Consortium project (Miller, et al., 2012). As with the CTM, the SLP measures the pavement profile using a laser, though the profile is linear rather than circular. Using analysis techniques outlined in ISO standards (ISO 13473-4 2008), MPD and root mean square (RMS) values are calculated, and used to determine the power spectral density (PSD). The PSD is a mathematical representation of the signal power distribution as a function of frequency. Spectral analysis methods based on signal processing techniques allow for characterization of the surface asperity distribution. Applying Discrete Fourier Transform (DFT) methods to surface profiles allows for calculation of PSD and texture

level distributions. Methods for acquiring and analyzing profile data will be detailed in the next chapter.
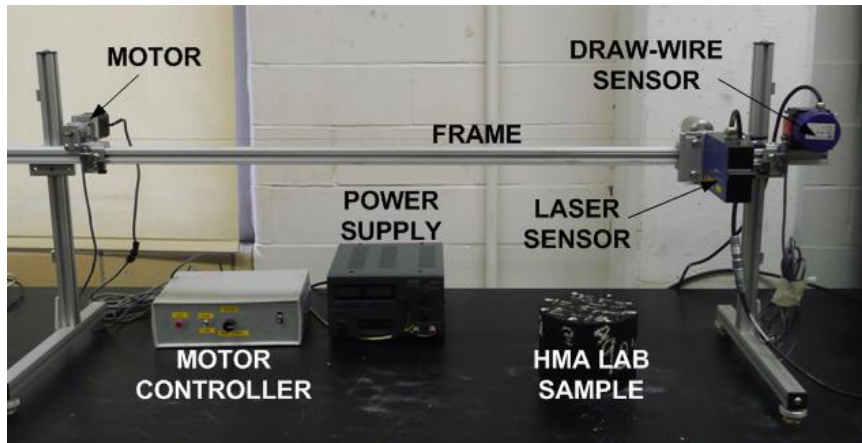
Figure 7. A Stationary Linear Profiler (SLP) evaluates micro-texture and macro-texture (Miller, et al., 2012).

Regression Analysis Approach

In this study, regression analysis was performed using Minitab16. MPD derived from SLP output was related to mixtures' volumetric and design properties, including bulk specific gravity (G_{mb}), air voids, binder content (P_b), and aggregate gradation properties including the nominal maximum aggregate size (NMAS), and gradation Weibull parameters, κ and λ. Weibull distribution which used to show the cumulative percent passing size of aggregates, has the form as shown in equation 3.

$$F(x, \kappa, \lambda) = 1 - e^{-\left(\frac{x}{\lambda}\right) \times \kappa} \tag{3}$$

where variable x is the aggregate size in millimeters, κ is the shape factor and λ is the scale factor (Masad, et al., 2009). A sample of cumulative Weibull distribution is shown in Figure 8. For this figure, the data points are the actual aggregate gradation while the curve is the Weibull distribution fitted to the data points for which κ is determined as 1.48 and λ is 1.59.
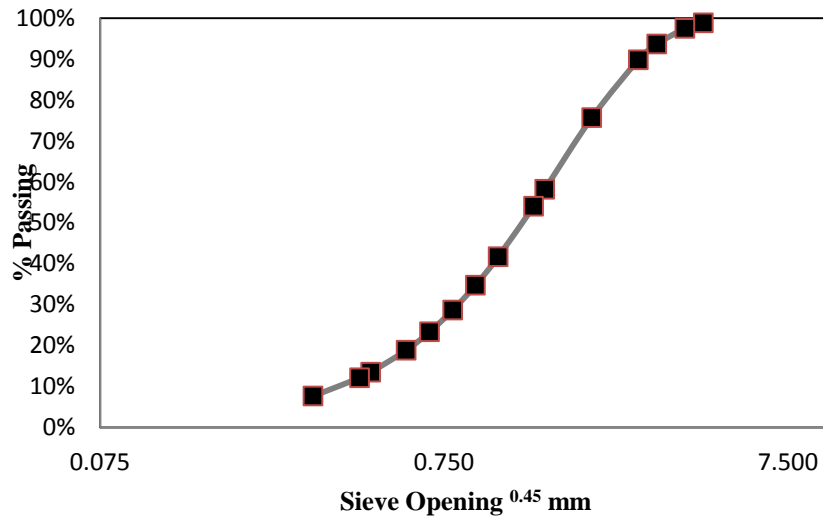
Figure 8. Cumulative Weibull distribution for aggregate gradation.

The statistical/regression models were developed for a wide range of selections of the aforementioned parameters.

Artificial Neural Networks (ANN) Approach

Researchers have used Artificial Neural Networks in many different aspects of civil engineering, particularly for situations in which the relationship between parameters becomes complicated and nonlinear. ANN is mainly used when proper relationships have not been established between input variables, large numbers of input variables exist, and the relationships between input and output of the model is rather complex. Thus ANN was deemed a suitable tool to model the relationship between surface texture, friction, and the mixture design parameters that can potentially affect these properties. ANN has been previously used in a number of pavement engineering studies, especially with regards to modulus back calculation and estimation (Bing, et al., 2002; Sakhaeifar, et al., 2010; Zofka & Yut, 2012).

ANN is a method mimics the neural system of human body means having several nodes and neurons. In this method, there are some layers (one input layer, several hidden layers and one output layer) containing nodes as shown in the Figure 9. These nodes in layers are connected to each other using lines. Each line is assigned a "weight" as an indicator of the effectiveness of that parameter in the output calculation. Several transfer functions are applied to input data to provide the output. Basic transfer functions can be listed as linear, exponential and hyperbolic tangent. Transfer functions are selected to minimize the number of the nodes in hidden layer because more nodes in the hidden layers results in more complicated network.
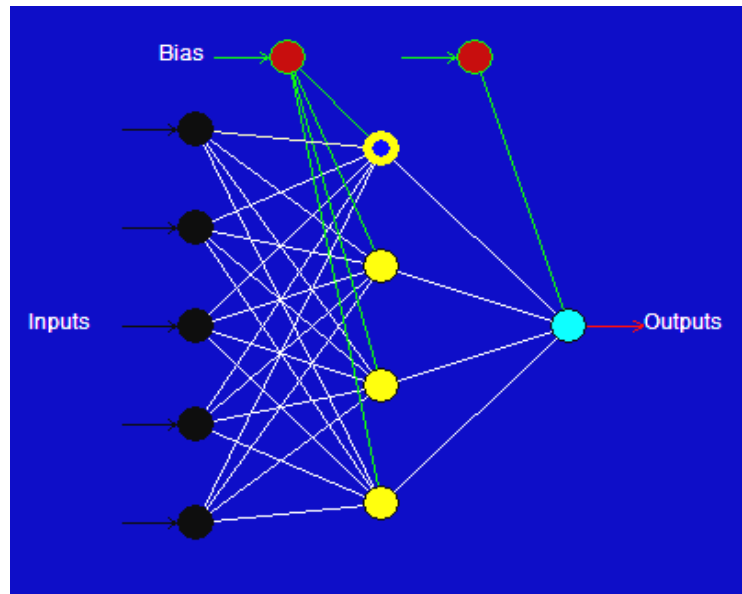
Figure 9. Artificial Neural Network diagram.

The model which is developed using ANN has three logical steps:multiplication, summation and activation. The dataset is randomly divided into two parts, 80 % of data are used for training the network and the remaining data is used to verify the developed network efficiency. Training the network will continue until the sum of squared errors between the model-predicted output and the experimentally measured output is minimized. The result of a network can be shown as a mathematical model contains weights, input, output, transfer function and bias.

From mathematical point of view, the ANN model can be shown as:

$$y(k) = F \left(\sum_{i=0}^{m} w_i(k) . x_i(k) + b \right) \qquad (4)$$

Where:
- m is the number of connection lines as shown in FIGURE 9,
- $x_i(k)$ is input value in discrete time k where i goes from 0 to m,
- $w_i(k)$ is weight value in discrete time k where i goes from 0 to m,
- b is bias,
- F is a transfer function,
- y(k) is output value in discrete time k.

More detailed information about ANN models can be found in several researches (Gurney, 1997; Kröse & Smagt, 1996; Rojas, 1996).

CHAPTER 3. METHODS AND MATERIALS

In this chapter, the analysis methods used to evaluate pavement surface texture and friction characteristics are described. Data processing techniques related to analysis of the texture spectrum are also discussed. Additionally, the field and laboratory materials used in the evaluation are mentioned.

DATA ACQUISITION METHODS

This study utilizes the results of three devices for measuring texture and friction. Friction devices are typically divided into those operating at highway speeds and those operating at low speeds or remaining stationary (Hall, et al., 2009). The texture devices are typically used to cover two primary texture ranges: macro-texture and micro-texture. Table 3 summarizes the devices, applicable test environments, and texture ranges.

Table 3. Summary of test devices, location, and texture range

Device	Location and Type	Texture Range
CTM (Circular Track Meter)	Field Texture	Macro-texture
SLP (Stationary Linear Profiler)	Field & Lab Texture	Macro-texture, Micro-texture

SLP Device Description

The SLP relies on the principle of optical triangulation to measure surface texture characteristics. A test frame supports the laser and draw-wire sensor devices on one end and a small motor at the other. The laser sensor projects a laser beam on the sample surface, which manifests as a red spot on the sample. The laser beam is diffusely reflected to an optical receiver array, which translates the light intensity of the reflected beam into an analog voltage signal that is then transformed into an amplitude measurement. The SLP triangulates surface amplitude as a motor pulls the laser assembly across the test frame at low speeds. Amplitude is coupled with horizontal displacement via the draw-wire sensor to define the surface profile. The combined amplitude-displacement measurement is registered in the computer's data acquisition card, which is transmitted to the software interface.

The laser used in this study is a CCD-type laser, model ILD 1700-40. Dimensions for the laser sensor are shown in Figure 10. Profiles are obtained from several different orientations in laboratory and field environments to reduce the effects of texture orientation on the overall response. Several parameters define the laser sensor's operational characteristics. Measuring range, measuring rate, sampling rate, resolution and spot diameter are some of the parameters used to characterize a laser sensor's operational capacity. Table 4 lists

relevant technical parameters related to the laser sensor's operation. ISO documentation outlines the technical requirements of the laser, and the reader should refer to these specifications for exact requirements in terms of horizontal and vertical resolution, sampling rate, and measuring rate (ISO 13473-3 2004). Data analysis templates can be configured to account for the various laser specifications.

Table 4. Summary of SLP Specifications

Spot Diameter (μm)	210
Measuring Range (mm)	40
Measuring Rate (Hz)	1250
Measuring Speed (mm/s)	37
Measuring Interval (points/mm)	15
Horizontal Resolution (μm)	4
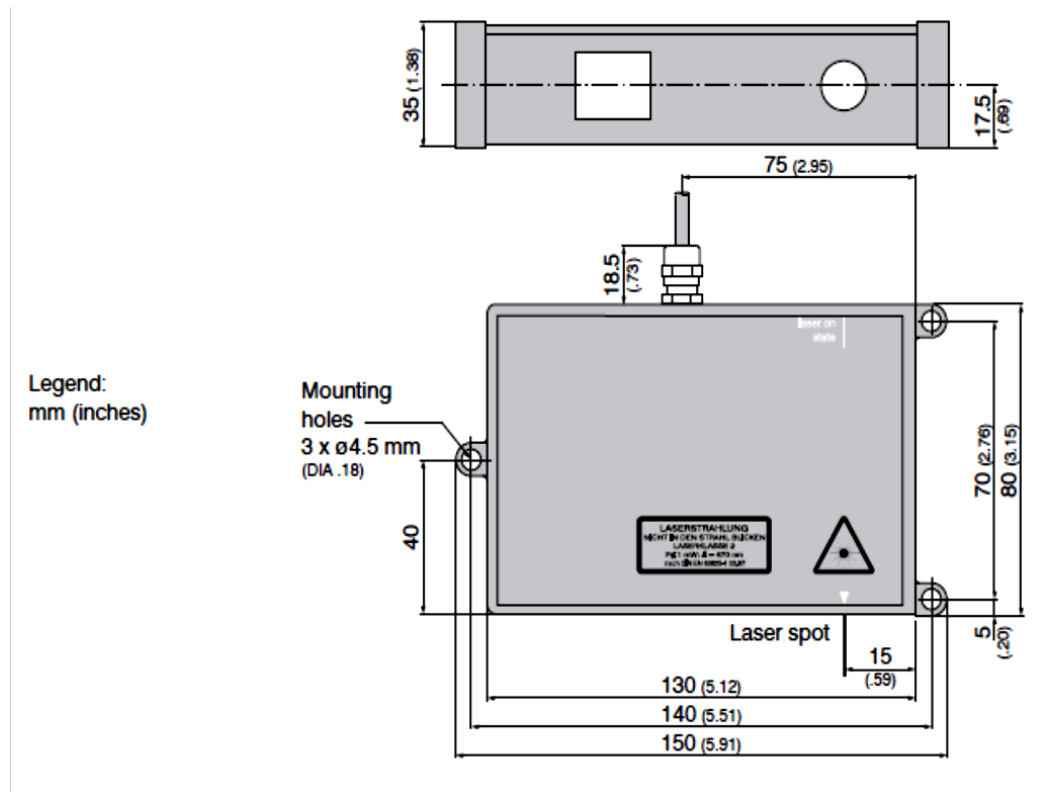
Legend:
mm (inches)

Mounting
holes
3 x ø4.5 mm
(DIA .18)

LASERSTRAHLUNG
NICHT IN DEN STRAHL BLICKEN
LASERKLASSE 2
P≤1 mW, λ = 670 nm
nach EN 60825-1:2001

Laser spot
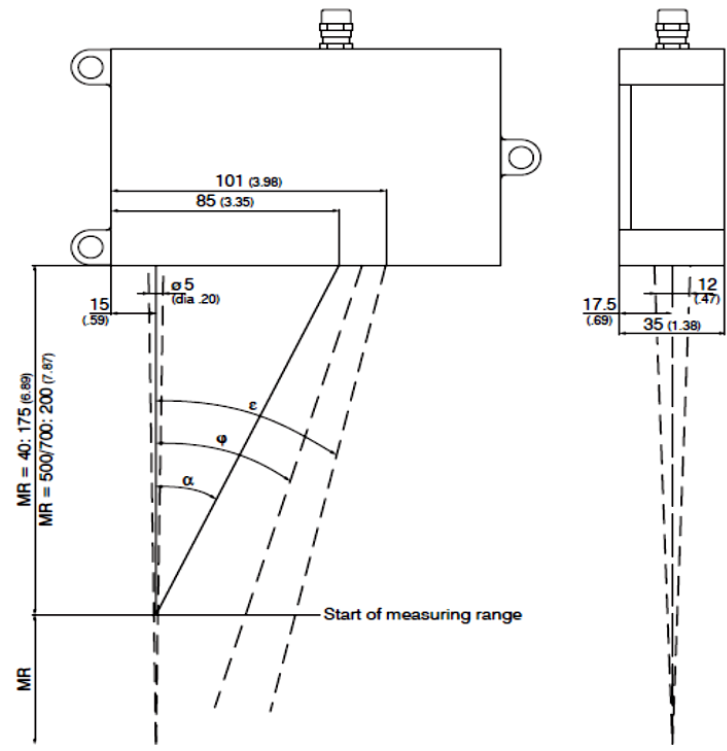
MR	α	φ	ε
40	22.1 °	21.9 °	21.8 °
500	19.3 °	9.8 °	7.0 °
750	19.3 °	7.7 °	5.0 °

Start of measuring range

Fig. 10 Free space for optics,
ranges 40/500/750 mm

Figure 10. Schematic diagrams of the ILD 1700-40 laser sensor.

20

The draw-wire sensor, also referred to as the displacement sensor or encoder, is configured to provide horizontal measurements at a fixed sampling rate. These readings coupled with amplitude measurements obtained from the laser sensor provide a two dimensional texture profile. In the test apparatus, the draw-wire sensor is physically attached to the laser sensor via a metallic cable that extends from the encoder housing as the laser sensor traverses the test frame. Care must be taken to ensure that the software is configured with the proper encoder settings for the particular laser model selected. Verification experiments can validate the accuracy of the laser sensor/encoder settings. The encoder model used in this research is a Micro-Epsilon WDS-1000-P60 sensor.

The test frame is outfitted with several clamps that allow for easy height and span adjustment. Height adjustment is critical because it ensures that the laser operates within its measuring range, which for this laser sensor/encoder combination is 40 mm. Manufactured on the UW-Madison campus, the test frame is made of industrial grade aluminum railing, though other suitably rigid materials may also be used. The frame includes height adjustors to ensure that the frame is level prior to testing. It is recommended to check that the frame is level and parallel to the roadway or laboratory mix surface by use of a hand level. Dimensions and specifications of the frame are available upon request.

The motor controller consists of a power switch, travel rate dial, and activation button. Low motor speeds and a lubricated rail are recommended to helpreduce vibrations of the laser and preserve the data integrity. A small piece of felt padding cushions the laser assembly as it retracts toward the encoder following data acquisition. Travel speed is regulated to ensure that motor operation does not introduce unnecessary vibrations to the laser sensor. Speed is adjusted using the travel rate dial. The exact speed at which the motor pulls the laser sensor across the test frame defines the measuring speed and depends on travel rate dial setting.

A standard power supply with adjustable voltage and amperage settings powers the laser sensor. The power supply is readily available commercially. Power settings for the laser sensor used in this research are limited to a maximum voltage of 24 V and a maximum current of 150 mA. Power requirements may differ for other lasers, so manufacturer recommendations must be consulted prior to operation. The greatest risk lies in overloading the laser with excessive electrical current, which can burn out the laser sensor and render the device inoperable. Because the laser is wired directly into the terminals of the power supply, care must be taken to ensure that the wire leads are properly attached to positive and negative terminals to avoid shorting out the device.

Additional data acquisition components are needed to couple laser sensor data with draw-wire sensor data. Both the laser sensor and draw-wire sensor feed into a PCI card that synchronizes data acquisition from the independent analog signals. The PCI card is housed internally in a desktop computer possessing appropriate DAQ card bays. Related software packages access the synchronized data for display and storage. The equipment manufacturer Micro-Epsilon developed the integrated software package that allows the PCI card to record laser/encoder displacement information. This research used the IF 2004 Encoder ILD 1700 V0.6 software application. A screenshot of the software application is shown in Figure .

The software is relatively simple to use, though special attention must be given to a few key fields to ensure proper data collection. The most convenient format for data output files is *.txt files. These files are easily opened in spreadsheet and analysis software programs. Data acquisition is triggered by the software upon activation of the motor controller and is terminated once the measurement is complete.
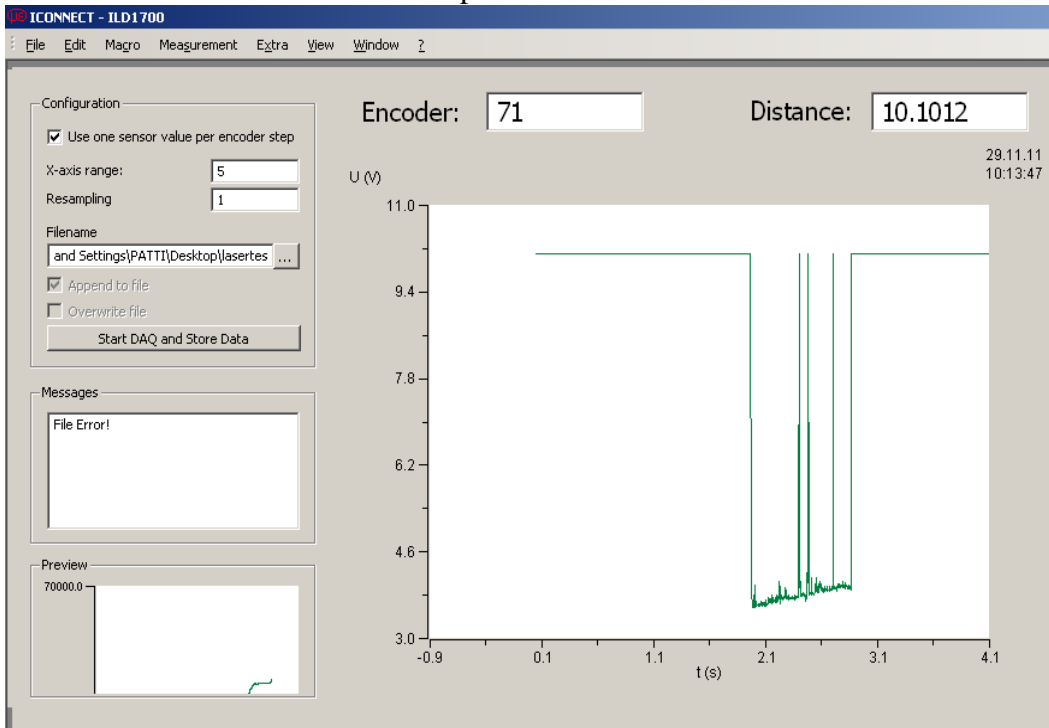
Figure 11. A screenshot from the software application used to collect SLP data.

Field evaluation requires a few additional components to account for a lack of alternating current electricity in field environments. These components supplement all of the components described previously. For power, a 12 V battery is used to power the laser sensor, motor controller, and data acquisition components. Deep-cycle batteries or similar types are recommended due to their extended discharge time. A battery charger should be used to charge the 12 V battery before and after field evaluations. A power inverter transforms 12 V direct current power from the battery to the 110 V alternating current needed by the test equipment. Because the PCI card requires a desktop computer for operation, a laptop could not be taken into the field for field evaluations. Future consideration could be paid to models that utilize smaller, portable PCI cards to enable efficient setup of data acquisition components and devices.

SLP Data Processing

After recording the raw surface profile with the SLP, several transformation algorithms are applied to the profile data. Data is imported into analysis spreadsheets as a *.txt file. Each file has two columns: the displacement count registered by the draw-wire sensor; and the

22

amplitude measurement recorded by the laser sensor. Removing invalid points, known as drop-outs, is the first priority in processing the profile (Haykin and Van Veen 1999). This is achieved in a three-step process. First, a device-dependent scale factor is applied to the raw profile data. In this case, the scale factor is 4. The scale factor is related to coordinate the measuring range of the laser and the capabilities of the software. In this case, the measuring range of the laser sensor is 40 mm and the software can accommodate a measuring range of 10 mm,thus the profile data must be scaled by a factor of 4. Applying this scale factor ensures that the analysis accounts for proper measuring range. In the second step, the profile is inverted to obtain a correct orientation. Once the profile is correctly oriented, the third step includes removing the drop-outs from the profile by applying a numerical drop-out threshold requirement. The occurrence of drop-outs increases with shiny surfaces and porous surfaces. After removing drop-outs, the profile is considered to be conditioned.

Conditioned data must satisfy the mathematical requirements of the Discrete Fourier Transform. Field data set is re-sampled at a 2-to-1 ratio to provide 2^{12} points or 4096 points. Resampling of laboratory data is not necessary, which utilizes 2^{11} points or 2048 points in the DFT analysis. Related sensitivity analyses indicate that resampling the field profile at a 2-to-1 ratio does not affect the texture level response due to the sufficiently high horizontal resolution of the laser. Higher resampling ratios may adversely affect the estimation of micro-texture as the sampling interval approaches the micro-texture spatial limit of 0.5 mm. While the selection of 2^{12} points represents the maximum number of points allowed in Microsoft Excel's Fourier Analysis package, other analysis packages such as Matlab may allow for a greater number of points to be processed and will increase data processing efficiency. In this study all analysis was conducted using Microsoft Excel spreadsheets.

Figure 17 shows representative profiles of dense and porous pavements. Both profiles have been conditioned and are ready for the next sequence of analysis algorithms. Note that the horizontal scale is five times greater than that of the vertical scale to accentuate differences in the profile type. Clearly the porous profile exhibits greater deviations in the amplitude, whereas the dense profile shows smaller perturbations along the surface. Being able to capture the distribution of these profile deviations is a primary advantage of using texture spectral analysis methods rather than other macro-texture indicators like mean profile depth (MPD). The method allows for characterization of the relative proportion of peaks and valleys, whereas MPD values provide an average of the amplitude magnitude in two or three dimensions, respectively. Likewise, micro-texture measurement methods such as the BPT and DFT fail to capture the distribution of smaller spatial wavelengths.
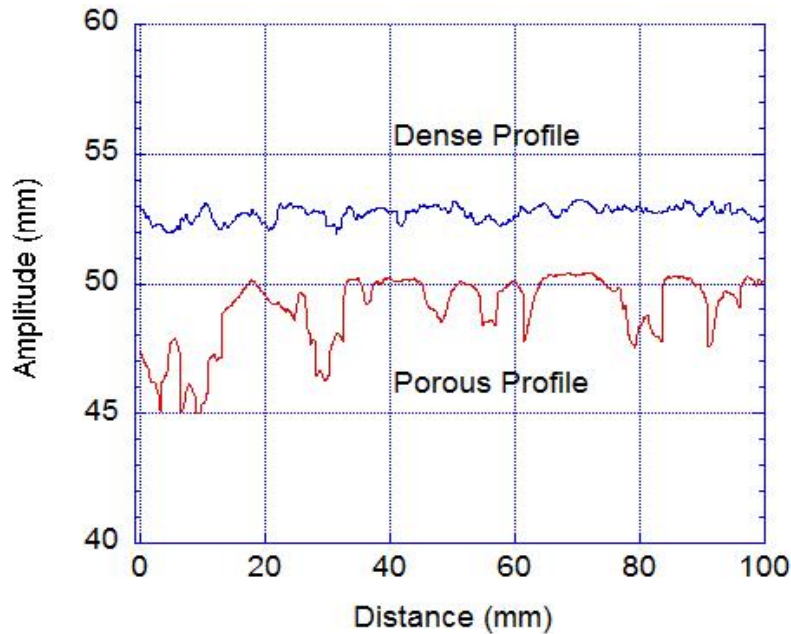
Figure 11. Profiles of dense and porous pavements.

Once the profile is conditioned and re-sampled, a second sequence of data transformations is applied. First, a least-squares fitting algorithm is used to achieve a slope of zero for the profile curve in a process known as slope suppression. Slope suppression eliminates a positive or negative profile slope that could affect the results of the DFT. Following slope suppression, the mean amplitude or y-intercept of the profile is set to zero in a process referred to as offset suppression. Following slope- and offset-suppression, the profile is subjected to a windowing algorithm to reduce the signal amplitude to zero at the edges of the profile. Windowing reduces signal leakage at profile edges. In this case, a Split Cosine Bell Window is an appropriate window since the profile is less than 1 m in length (ISO 13473-4 2008). Other windows are specified in related ISO standards and may be appropriate for other evaluation systems. Once the profile is windowed, the Discrete Fourier Transform can be applied to determine the texture level distribution.

Using techniques outlined in related ISO standards, MPD values are calculated along with the power spectral density (PSD). The Discrete Fourier Transform translates the random surface profile into a series of complex sinusoidal waveforms. Coefficients arising from the Discrete Fourier Transform are associated with complex sinusoids of different frequencies (ISO 13473-2 2002). This series of waveforms forms the basis of the PSD, which defines the distribution of waveforms for the profile over a wide range of frequencies. The amplitude and texture level distributions originate from the power spectral density (PSD). The texture level distribution provides a more detailed metric by which to evaluate texture. This procedure follows the methods articulated by Losa et al and has been updated to meet the research needs of this study (Losa et al 2005, Losa et al 2007, Losa & Leandri 2010).

The texture level distribution estimates the proportion of particular wavelengths in the profile, which can be attributed to aggregate and mixture properties and related to frictional

characteristics. These wavelengths are captured in spectral bands of different widths called octave bands. The center wavelength of each octave band is represented by the symbol λ. Octave bands are calculated as 2^n, where n is an integer. For each octave band, the Discrete Fourier Transform calculates the root mean square (RMS) value of the surface profile amplitude, symbolized as a_λ. A reference root mean square value (a_{ref}) of 10^{-6} m is assumed per the ISO 13473-4 standard. The texture profile level (L_{TX}), which is measured in decibels (dB), is calculated as:

$$L_{TX} = 10 \times \log\frac{a_\lambda{}^2}{a_{ref}{}^2} \tag{5}$$

Four profiles are recorded for each laboratory SGC sample and field testing zone. Individual profiles for each sample are averaged using a geometric mean formulation for a specified octave band according to the following equation:

$$L_{TX,\lambda}^{mean} = 10 \times \log(\frac{10^{\frac{L_{TX,\lambda}^1}{10}} + 10^{\frac{L_{TX,\lambda}^2}{10}} + 10^{\frac{L_{TX,\lambda}^3}{10}} + 10^{\frac{L_{TX,\lambda}^4}{10}}}{4}) \tag{6}$$

Once the mean texture level ($L_{TX,\lambda}^{mean}$) for a given octave band is known, texture parameters can be constructed from any combination of the octave bands. The series of octave bands encompassing the micro-texture and macro-texture wavelength ranges can be represented as $L_{TX,\ 0.5\text{-}32}$. Note that the λ values indicated in this parameter correspond to the central wavelength in the octave band, though the actual bandwidth is characteristically larger since the limits of the octave band extend beyond this central wavelength. For the micro-texture/macro-texture indicator $L_{TX,\ 0.5\text{-}32}$, the band corresponds to wavelengths ranging from $0.4 - 40.3$ mm. The formula for calculating this texture parameter range is given in:

$$L_{TX,\ i \to j} = 10 \times \log(\sum_{\lambda=i}^{j} 10^{\frac{L_{TX,\lambda}^{mean}}{10}}) \tag{7}$$

Mean profile depth (MPD) values can be calculated from the profile by following the procedure articulated in ISO 13473-1. Using an evaluation length of 100 mm, a series of high-pass and low-pass filters are applied to the profile to remove low-frequency and high-frequency content. The high-pass filter removes texture wavelengths greater than 100 mm. After high-pass filtering, a low-pass filter is applied to the profile to remove frequencies corresponding to texture wavelengths less than 2.5 mm. The evaluation length of 100 mm is divided into two equal halves. In each 50 mm section, the highest peak is determined. The MPD value represents the arithmetic average of the two peak values minus the average profile amplitude.

MATERIALS

In this study, researchers selected field samples from the Wisconsin Highway Research Program (WHRP) and the Minnesota Department of Transportation pavement test track facility (MnROAD) for laboratory texture measurement and use of field friction data and measures. Additionally, data previously collected from a Wisconsin Highway Research Program (WHRP) project and as part of the Asphalt Research consortium was also used in the analysis and modeling effort conducted in the present study.

Friction data from the CTM and Friction Number tests, as well as the corresponding mixture design information from 14 MnROAD cells were considered in the present study. Cores from a number of these sections were acquired and used for derivation of laboratory texture measurements using the SLP. The properties of the MnROAD sections considered in this study are shown in Table 5.

Table 5. Characteristics and Properties MnROAD Sections and field cores

MnROAD CELL/Section	Bulk Specific Gravity (Gmb)	VTM (%)	NMAS (mm)
1*	2.37	4.07	12.5
2	2.34	4.23	12.5
3	2.36	4.22	12.5
4	2.37	4.39	12.5
19*	2.34	3.53	12.5
22	2.36	3.83	12.5
24	2.36	3.66	12.5
27	2.35	3.34	12.5
31*	2.36	3.89	12.5
33*	2.38	4.60	12.5
34*	2.39	3.98	12.5
77*	2.37	4.50	12.5
86	2.02	19.90	12.5
87	2.36	4.90	12.5

Field cores tested in laboratory

The cores from the WHRP study (Project ID 0092-12-02) contained reclaimed asphalt pavement (RAP) and warm mix additives. Samples consisted of three different NMAS and a single binder type. Sample characteristics for the field cores are given in Table 6.

Table 6. Characteristics of the WHRP (Project ID 0092-12-02) field core sample set

Roadway	Aggregate Type	NMAS (mm)	Design ESALs	PG Grade	RAP/RAS Content
USH 41	Gravel	19.0	E-10	58-28	8%
USH 41	Gravel	12.5	E-3	58-28	17%
USH 41	Gravel	12.5	E-10	58-28	8.5%
USH 41	Gravel	25.0	E-1	58-28	13%

Additionally, data collected from an earlier Wisconsin Highway Research Program (WHRP) project and as part of the Asphalt Research consortium was also used in the analysis and modeling effort conducted in the present study. Sample characteristics for the field cores are given in Table 7 (WHRP0092-12-02, 2011). Samples originated from a variety of roadways from counties across Wisconsin.

Table 7. Characteristics of the WHRP field core sample set

Roadway	County	Aggregate Type	NMAS (mm)	Design ESALs	PG Grade
US 8	Oneida	Gravel	12.5	E-3	58-28
US 18	Iowa	Limestone	12.5	E-3	64-22
US 18	Milwaukee	Limestone	12.5	E-3	64-22
STH 32	Racine	Limestone	19.0	E-3	64-22
STH 33	La Crosse	Limestone	19.0	E-1	58-28
IH 39	Marquette	Gravel	12.5	E-10	58-28
IH 39	Portage	Gravel	12.5	E-10	58-28
US 41	Fond du Lac	Limestone	12.5	E-30	64-22
STH 44	Fond du Lac	Limestone	12.5	E-1	58-28
US 45	Langlade	Gravel	12.5	E-3	58-28
US 53	Chippewa	Gravel	12.5	E-10	58-28
US 53	Chippewa	Gravel	19.0	E-10	58-28
US 53	Chippewa	Gravel	25.0	E-10	58-28
US 53	Trempealeau	Limestone	12.5	E-3	64-22
STH 57	Brown	Limestone	12.5	E-3	58-28
STH 59	Waukesha	Limestone	19.0	E-3	64-22
STH 60	Richland	Limestone	19.0	E-1	64-22
STH 60	Washington	Gravel	19.0	E-10	64-28
STH 67	Waukesha	Limestone	19.0	E-1	58-28
STH 70	Vilas	Gravel	12.5	E-1	58-28
STH 77	Ashland	Gravel	12.5	E-1	58-28
STH 96	Waupaca	Limestone	12.5	E-3	58-28
STH 153	Marathon	Gravel	12.5	E-3	58-28
STH 181	Milwaukee	Limestone	12.5	E-10	64-22
STH 181	Milwaukee	Limestone	19.0	E-10	64-22

Note: US: US Highway. STH: State Trunk Highway, IH: Interstate Highway

Furthermore data collected during the ARC project from field site locations across Dane county was added to the dataset, as shown in Figure 12. Mix design information, site access, and material sampling assistance were provided by four local contractors. Researchers collected friction data at the project locations. Participating contractors largely dictated the location of field evaluations used in this dataset.
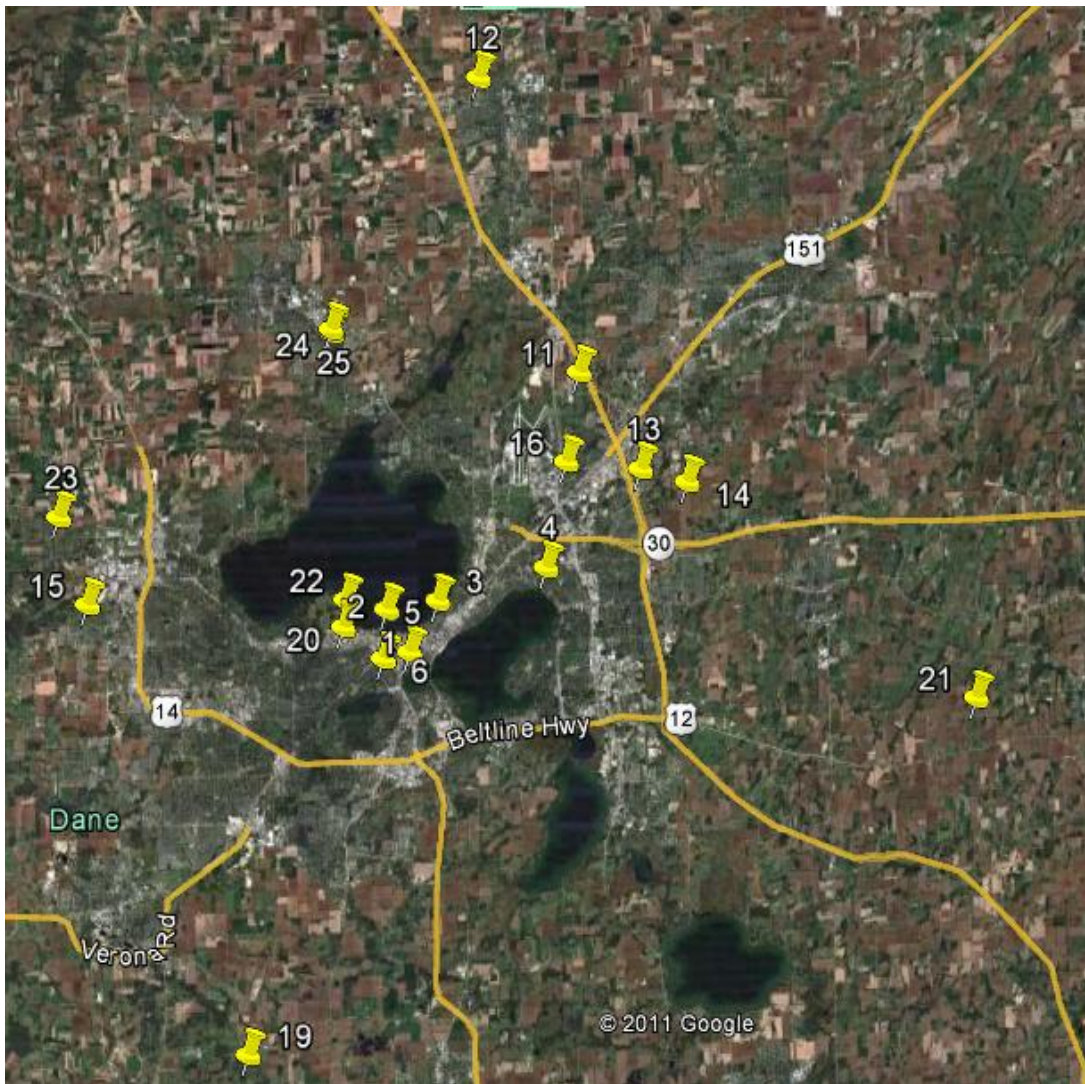
Figure 12. Locations of field test sites in Dane County.

Selected sites comprised a range of mixture design characteristics, which are expected to manifest in a wide spectrum of surface texture properties. At each field site, researchers used the five test methods described previously to evaluate pavement surface texture and frictional characteristics. These sites encompassed low-volume roads and parking lots in order to reduce traffic interruptions and to ensure the safety of the field evaluation crew. At each site, the field evaluation crew demarcated two data collection zones and followed standard American Society for Testing and Materials (ASTM) procedures to collect a

sufficient number of samples (ASTM E1911 2009, ASTM E2157 2009). Data collected from each zone is averaged to obtain an aggregated site value. CTM and SLP tests, among other tests, were conducted in these locations.

CHAPTER 4. RESULTS AND ANALYSIS

Selection of Laboratory Texture Analysis Parameter

An important prerequisite of input variables used for both statistical and artificial neural network (ANN) modeling to predict pavement texture/friction characteristics is statistical independence of the input variables. As previously discussed, the SLP provides three output parameters, the mean profile depth (MPD), L_{TX2-4}, and L_{TX4-32} (as defined by equation 6). In order to make an appropriate selection of parameters to be used for modeling purposes in the present study, statistical correlations were developed between the aforementioned laser output parameters, as shown in Figure 13. The results show that strong statistical correlations exist between all three possible pairs of parameters, indicating that no more than one of these parameters is necessary to be used in any given modeling process. Thus MPD was selected for subsequent analysis and modeling purposes, in part due to the relative simplicity of establishing physical relationships between this parameter and friction and mixture design parameters.

The relationship between laboratory measurement of pavement surface texture based on the mean profile depth parameter (MPD) (measured using the SLP device) and mix design and volumetric properties was assessed using regression analysis. This statistical model was based on predominantly aggregate-driven parameters (i.e. NMAS, κ, λ), resulting in a very good correlation between model predicted and the SLP-measured MPD values, (R-squared value of 78%), as shown in Figure 14. As it is shown in the figure, there are three points far from others. These points are porous asphalt mixtures. By removing these data the R-squared is reduced to 60 %. It should be noted that by incorporating the data corresponding to porous mixtures, the effect of aggregate gradation characteristics is magnified due to the larger range of κ and λ values, thus when the porous mixtures data are removed and the data set is reduced to dense graded mixtures, the significance of gradation parameters is reduced.

The magnitude of the statistical parameter, p-value, for each variable used in the regression model is an indicator of the significance of that variable, with values closer to zero indicating the highest significance while the significance of values approaching 1.0 is negligible. The P-values for factors used in regression analysis are shown in Table 8.

(a)

(b)

(c)
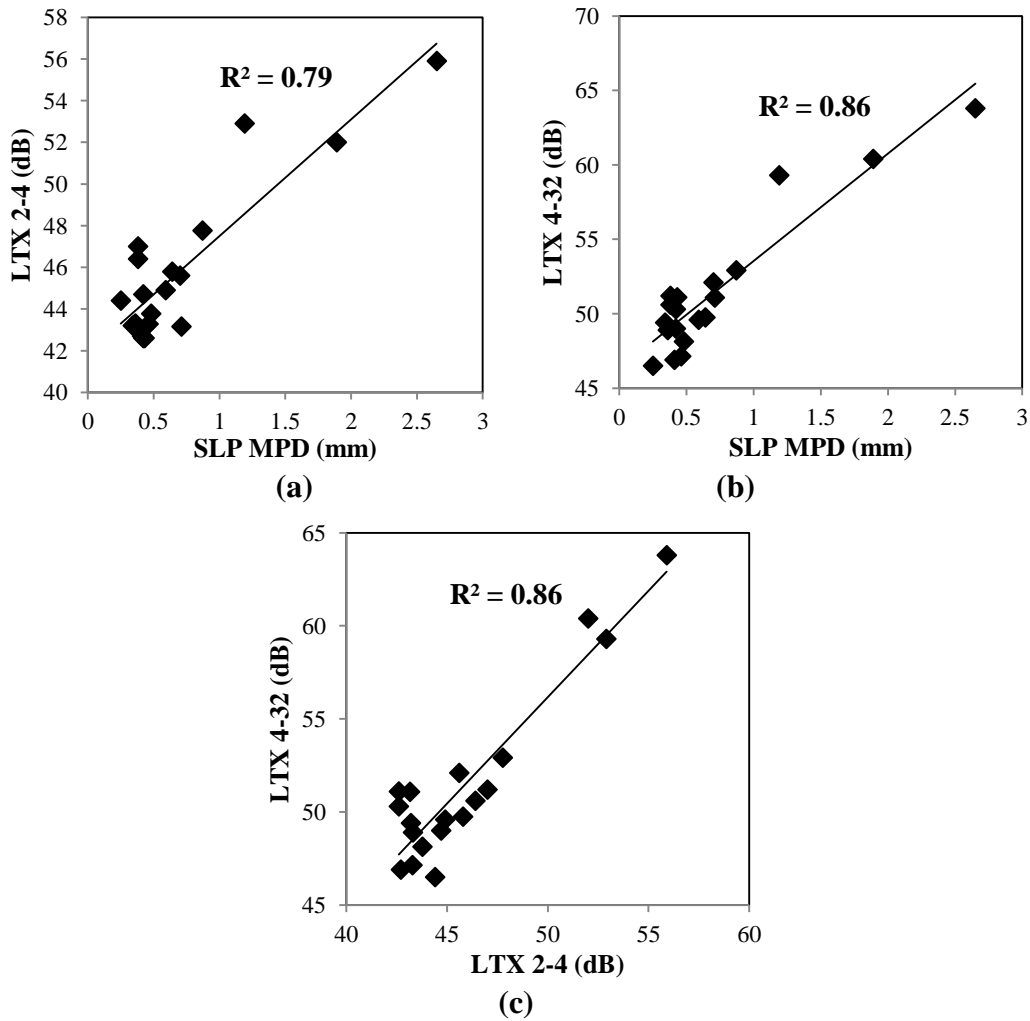
Figure 13. Assessment of statistical independence of Laser Profilometer output parameters.

Table 8. values for the Statistical Model Parameters

Predictor	Coefficient	Standard Error Coefficient	T value	P value
Constant	9.467	4.040	2.340	0.036
G_{mb}	-3.197	1.115	-2.870	0.013
P_b	-0.356	0.315	-1.130	0.278
NMAS	0.085	0.043	1.940	0.074
κ	1.354	0.234	5.800	0.000
λ	-1.476	0.360	-4.100	0.001

The regression model equation is shown below:

$$\text{Laser MPD} = 9.47 - 3.20\ G_{mb} - 0.356\ P_b + 0.0846\ \text{NMAS} + 1.35\ \kappa - 1.48\ \lambda \qquad (8)$$

Where MPD is the mean profile depth in millimeter, G_{mb} is bulk asphalt mixture density (g/cm^3), P_b is the binder percent, NMAS is the nominal maximum aggregate size in millimeter, κ and λ are the Weibull distribution parameters.
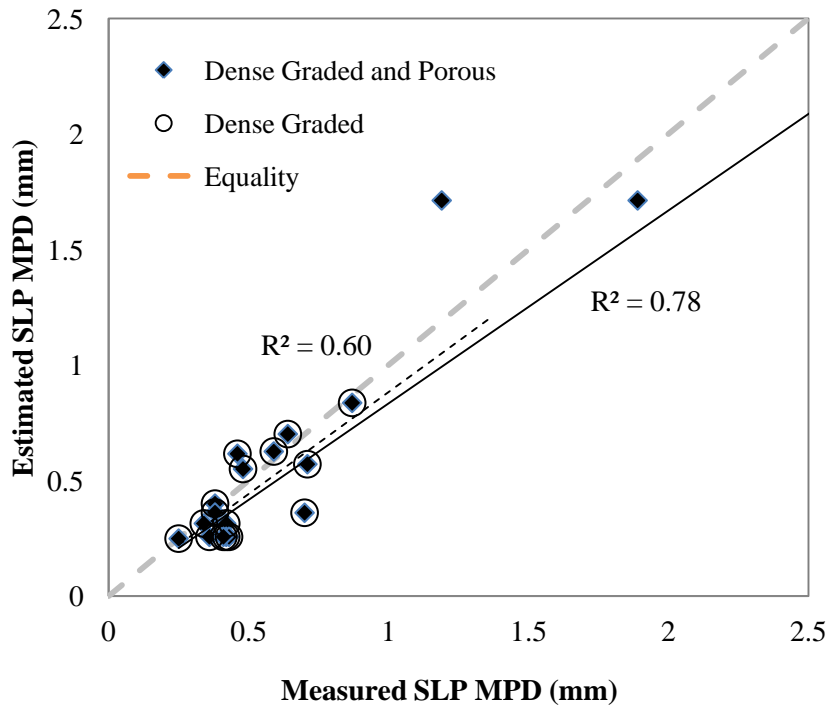
Figure 14. Estimated MPD versus measured MPD from SLP device.

Based on the p-value analysis, the model predictions are most dependent on the Weibull distribution parameters (κ and λ). These parameters are indicators of the shape of the gradation curve, thus the high significance of these variables indicates the close dependency of the pavement friction to the aggregate gradation. The positive coefficient of κ and the negative coefficient of λ in the model indicate that increasing κ and decreasing λ will result in higher MPD values and thus improved pavement friction.

Higher κ values will result in gradations closer to a more one-sized gradation, and further from the maximum density line, while decreasing λ will generally result in finer gradation. With regards to the trend of λ, it hypothesized that what is important is how far the gradation curve is from the maximum density line, rather than the overall coarseness or fineness of the gradation. A gradation curve far from the maximum density line on the coarse side, will likely have a higher MPD compared to a gradation curve which is far from maximum density line on the finer side. To prove this hypothesis, the gradation curves of

32

the mixtures in this study are compared with the maximum density line in Figure 15. It is observed that all gradation curves fall above the maximum density line. In such conditions decreasing the value of λ will result in curves further from the maximum density line (i.e. lower aggregate packing) and thus believed to provide a higher texture. This trend explains the appropriateness of the negative coefficient of λ in equation 8.
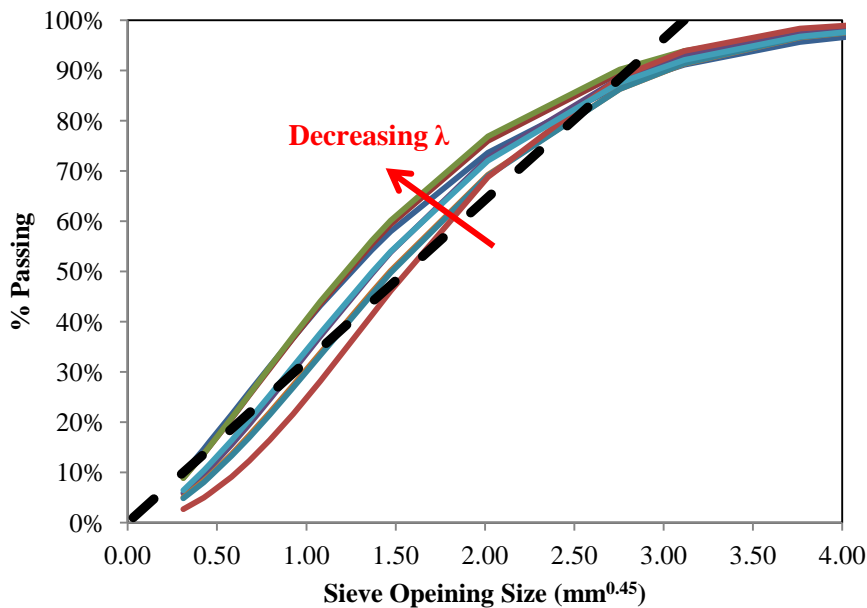
Figure 15. Effect of λ on distance of mixture gradation curves from the maximum density line.

Another aggregate gradation parameter of high significance in the regression model is the Nominal Maximum Aggregate Size (NMAS), which is the sieve size immediately above the first sieve retaining more than 10% of the aggregates. The positive coefficient in the model indicates that gradations with higher NMAS thus generally coarser gradations result in higher MPD and subsequently increase the texture.

This model is also closely related to the bulk specific gravity (G_{mb}) which signifies the bulk asphalt concrete density including the air voids. Thus the negative coefficient of G_{mb} in the regression model indicates that a lower G_{mb}, which results in higher porosity, leads to higher MPD and texture consequently.

Furthermore, a dependency also exists between P_b (i.e. binder content) and MPD, although the significance is relatively weaker than that of the gradation and density variables. The negative coefficient indicates that lower P_b will increase the expected texture, possibly by reducing binder film thickness around aggregates as well as reducing the aggregate packing level in mixture during compaction.

To verify the results from the regression analysis, ANN modeling was performed using the same dataset. For this model, the input variables were selected as G_{mb}, P_b, NMAS, κ and λ

based on statistically significant contibutors to prediction of e MPD, predictions were compared to actual MPD values from laser measurements. The transfer function used in the hidden layer was selected to minimize the nodes in hidden layer, in this case the hyperbolic tangent function, as shown in equation 9.

$$tanh x = \frac{e^x - e^{-x}}{e^x + e^{-x}} \quad\quad\quad (9)$$

where x is the input (variable).

The network model calibration or "training" data set consisted of 80 % of the data set, while the remaining 20% were randomly selected for use as model verification ("test" dataset), and thus were not used for model training. Model optimization was performed using the training data set to derive the weights of each node connection and the network bias values, as listed in Table 9. The optimized nodal parameters predicted the training output values with a high R-squared of 97 %. For model verification, the model was applied to the randomly selected test dataset which resulted in a relatively good R-squared value of 71 %, thus verifying the accuracy of the developed ANN model.

Table 9. Weights of Each Nodes in ANN Model Output

Nodes	Weight	Nodes	Weight	Nodes	Weight
N1L1-N1L2	1.7564	N3L1-N3L2	-0.0857	N1L2-N1L3	-3.4413
N1L1-N2L2	2.2794	N3L1-N4L2	1.9725	N2L2-N1L3	3.4841
N1L1-N3L2	-0.9449	N4L1-N1L2	2.9717	N3L2-N1L3	1.4798
N1L1-N4L2	-0.2728	N4L1-N2L2	0.7685	N4L2-N1L3	-3.5754
N2L1-N1L2	-1.0398	N4L1-N3L2	-1.5427	B1-N1L2	1.4369
N2L1-N2L2	-3.7149	N4L1-N4L2	-4.6293	B1-N2L2	0.2504
N2L1-N3L2	0.0439	N5L1-N1L2	-0.1939	B1-N3L2	0.2228
N2L1-N4L2	-1.3159	N5L1-N2L2	-1.5465	B1-N4L2	-1.2515
N3L1-N1L2	-0.7391	N5L1-N3L2	0.587	B2-N1L3	0.5153
N3L1-N2L2	2.8365	N5L1-N4L2	1.4941		

Relating Field Friction Tests to Laboratory Laser Measurements
In order to develop a relationship between field and laboratory friction measures, the smooth tire friction number (FN) measured at 65 km/hour was used. Field measured values of CTM and SLP MPD is used to develop relation between texture measurement results and friction (i.e. FN). Using this data and the developed database in this study, the relationships shown in Figure 16 are observed. This leads to the use of a three-step process for relating SLP measured MPD to field FN, as is discussed below.
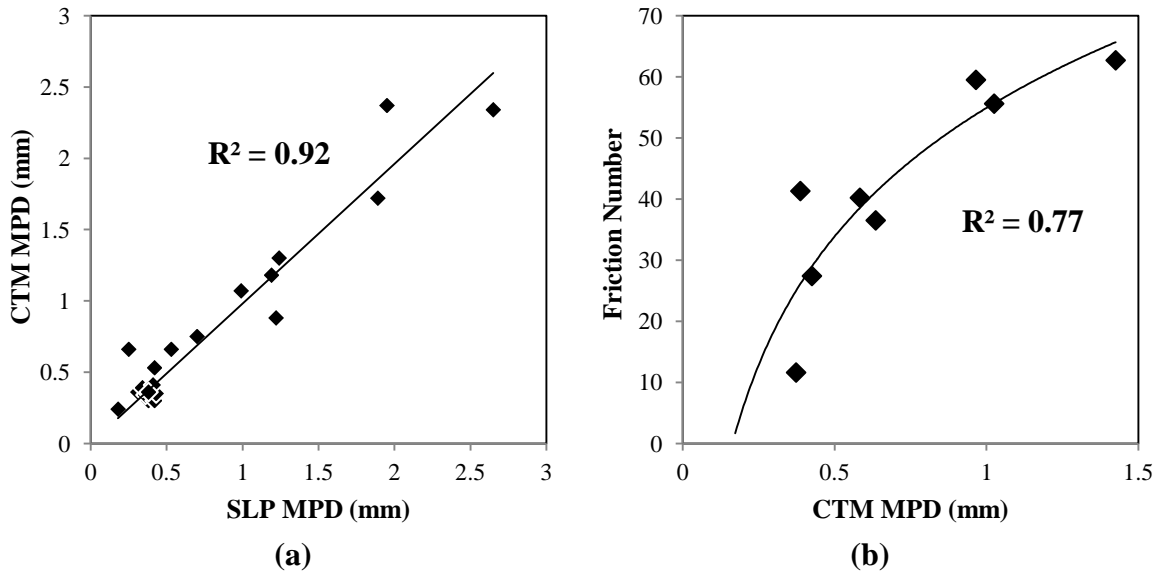
Figure 16. (a) Relationship between CTM MPD from field and SLP MPD from laboratory; (b) Relationship between smooth-tire Friction Number from field and CTM MPD.

First using the strong relationship between CTM-measured MPD from field and the SLP-measured MPD from laboratory compacted loose mix samples developed in Figure 16(a), equation 10 was derived, by setting a zero intercept:

$$CTM\ MPD = 0.98 \times (SLP\ MPD) \tag{10}$$

Where:
- CTM MPD is the mean profile depth (mm) measured using the CTM in the field,
- SLP MPD is the mean profile depth (mm) measured using the laser profilometer in the laboratory.

In the second step, a significant nonlinear relationship was established between FN and the CTM MPD (Figure 16(b)), resulting in equation 11:

$$FN = 30.362 \times \ln(CTM\ MPD) + 54.912 \tag{11}$$

Where:
- FN is the smooth-tire friction number from field measurements,
- CTM MPD is the mean profile depth (mm) measured using the CTM in the field.

Finally by combining the two relationships, laboratory SLP MPD measures were directly related to the field FN results. The resulting relationship is shown in equation 12:

$$FN = 30.362 \times \ln(SLP\ MPD) + 54.299 \tag{12}$$

Where:

- FN is the smooth-tire friction number from field measurements,
- SLP MPD is the mean profile depth (mm) measured using the laser profilometer in the laboratory.

The relationship derived in equation 12 shows how laboratory measures can be directly related to field friction values, with the positive coefficient of the SLP MPD parameters indicating that increasing texture mean profile depth will results in increased field friction. Furthermore, extending the direct strong relationships observed in Figure 13(a) and (b), it can be further inferred that increasing L_{TX2-4} and L_{TX4-32} will also result in increasing field friction numbers. Thus using the relationships developed in this study in which mixture design parameters (i.e. volumetric and aggregate gradation properties) were related to laboratory texture measures, one may consequently adjust the pavement mixture design in the laboratory to achieve target texture and field friction measures.

CHAPTER 5. FINDINGS AND RECOMMENDATIONS

SUMARY OF FINDINGS

In this study, statistical and artificial neural network modeling was performed using surface texture and friction parameters measurements from laboratory- and field-based devices including the Stationary Laser Profilometer (SLP), Circular Track Meter (CTM) and Locked-wheel smooth tire device. The following findings have been observed:

- Using statistical analysis and artificial neural network modeling, mixture design parameters (i.e. volumetric and aggregate gradation properties) could be related to laboratory texture measurements (MPD). Therefore, knowing mixture design properties can lead to the estimation of road texture parameters.
- It is shown that pavement texture is mainly controlled by aggregate gradation and mixture volumetric characteristics. Additionally, it was shown that increasing the distance of the gradation curve from the maximum density line is more important than the overall coarseness or fineness of the gradation in terms of increasing the expected texture.
- Laboratory measured friction parameters (MPD) can be related to field friction values (FN) using regression analysis.
- Utilizing the models developed in this study, by further investigation, mixture designers can have a guideline to estimate friction.
- Models developed in this study showed that the measurements for field and laboratory compacted samples from SLP device can be used to estimate friction parameters.

RECOMMENDATIONS FOR FUTURE WORK

Because the models developed in this study utilized a limited data set, more mixes are needed to verify the models and validate the model coefficients. While the data set presented here is encouraging, disseminating the SLP device specification and analysis method to other research labs may improve the method.

Additional model parameters may allow for improved estimation of texture characteristics, however, further experimentation on laboratory samples with controlled gradations is necessary for establishing clearer relationships between lab and field compacted texture characteristics. Additionally, a comprehensive study can show the effect of polishing and aggregate wearing in field on tire-pavement friction throughout pavement life.

ACKNOWLEDGMENTS

The results and opinions presented are those of the authors and do not necessarily reflect those of the sponsoring agencies.

REFERENCES

1.   AASHTO, 1976. *Guidelines for Skid-Resistant Pavement Design,* Washington, D.C.: American Association of State Highway and Transportation Officials.

2.   Ahammed, M. & Tighe, S., 2009 . Early-Life, Long-Term, and Seasonal Variations in Skid Resistance in Flexible and Rigid Pavements. *Transportation Research Record: Journal of the Transportation Research Board,* Volume No. 2094, pp. pp. 112-120.

3.   Ahammed, M. and Tighe, S. "Asphalt Pavement Surface Texture, Friction, and Noise: Findings from CPATT Quiet Pavement Research." National Sciences and Engineering Research Council (NSERC), Canada, 2008.

4.   Ahammed, M. and Tighe, S. "Early-Life, Long-Term, and Seasonal Variations in Skid Resistance in Flexible and Rigid Pavements." *Transportation Research Record: Journal of the Transportation Research Board, No. 2094, Transportation Research Board of the National Academies,* Washington, D.C., 2009, pp. 112-120.

5.   ASTM. Standard Practice for Calculating Pavement Macrotexture Mean Profile Depth. Standard No. E1845*, American* Society for Testing and Materials, West Conshohocken, PA, 2009.

6.   ASTM. Standard Test Method for Measuring Paved Surface Frictional Properties Using the Dynamic Friction Tester, Standard No. E1911, American Society for Testing and Materials, West Conshohocken, PA, 2009.

7.   ASTM. Standard Test Method for Measuring Pavement Macrotexture Depth Using a Volumetric Technique, Standard No. E965, *American Society for Testing and Materials*, West Conshohocken, PA, 2006.

8.   ASTM. Standard Test Method for Measuring Pavement Macrotexture Properties Using the Circular Track Meter, Standard No. E2157, *American Society for Testing and Materials*, West Conshohocken, PA, 2009.

9.   ASTM. Standard Test Method for Measuring Surface Frictional Properties Using the British Pendulum Tester, Standard No. E303, American Society for Testing and Materials, West Conshohocken, PA, 2008.

10.   Bing, X., Ranjithan, S. R. & Kim, Y. R., 2002. New Condition Assessment Procedure for Asphalt Pavement Layers, Using Falling Weight Deflectometer Deflections. *Transportation Research Record 1806.*

11.   Flintsch, G., de Leon, E., McGhee, K., and Al-Qadi, I. "Pavement Surface Macrotexture Measurement and Applications." *Transportation Research Record: Journal of the Transportation Research Board, No. 1860, Transportation Research Board of the National Academies,* Washington, D.C., 2003, pp. 168-177.

12. Flintsch, G., Huang, M., and McGhee, K. "Harmonization of Macrotexture Measuring Devices." *Journal of ASTM International,* American Society of Testing and Materials, 2(9), 2005.

13. Giles, C.G., Sabey, B.E., and Cardew, K.H.F. "Development and Performance of the Portable Skid Resistance Tester." American Society for Testing and Materials (ASTM), ASTM Special Technical Publication No. 326, Philadelphia, Pennsylvania, 1962.

14. Gurney, K., 1997. *An Introduction to Neural Networks.* London: Routledge, ISBN 1-85728-673-1.

15. Hall, J. et al., 2009. *Guide for Pavement Friction,* s.l.: NCHRP Web Only Document.

16. Hall, J.W., Smith, K.L., Titus-Glover, L., Wambold, J.C., Yager, T.J., and Rado, Z. "Guide for Pavement Friction." National Cooperative Highway Research Program, Project 01-43, Washington, DC, 2009.

17. Hanson, D. & Prowell, B., 2004. *Evaluation of Circular Texture Meter for Measuring SurfaceTexture of Pavements,* Auburn, AL: National Center for Asphalt Technology.

18. Haykin, S. and Van Veen, B. "Signals and Systems." John Wiley & Sons, New York, 1999.

19. Henry, J. J., 2000. National CooperaEvaluation of Pavement Friction Characteristics: A Synthesis of Highway Practice, Washington, DC: National Cooperative Highway Research Program.

20. ISO. Characterization of Pavement Texture by Use of Surface Profiles – Part 1: Determination of Mean Profile Depth, Standard No. 13473-1, *International Organization for Standardization*, 2004.

21. ISO. Characterization of Pavement Texture by Use of Surface Profiles – Part 2: Terminology and Basic Requirements Related to Pavement Texture Profile Analysis, Standard No. 13473-2, *International Organization for Standardization*, 2002.

22. ISO. Characterization of Pavement Texture by Use of Surface Profiles – Part 3: Specification and Classification of Profilometers, Standard No. 13473-3, *International Organization for Standardization*, 2004.

23. ISO. Characterization of Pavement Texture by Use of Surface Profiles – Part 4: Spectral Analysis of Texture Profiles, Standard No. 13473-4, *International Organization for Standardization*, 2008.

24. Ivan, J. et al., 2010. *Incorporating Wet Pavement Friction into Traffic Safety Analysis,* Storrs, CT: Connecticut Department of Transportation.

25. Kröse, B. & Smagt, P., 1996. *An Introduction to Neural Networks.* Amsterdam: The University of Amsterdam.

26. Kuttesch, J. S., 2004. *Quantifying the Relationship Between Skid Resistance and Wet Weather Accidents for Virginia Data,* Blacksburg, Virginia.: M.S. Thesis, Department of Civil Engineering, Virginia Polytechnic Institute and State University.

27. Losa, M., and Leandri, P. "The Reliability of Tests and Data Processing Procedures for Pavement Macrotexture Evaluation." *International Journal of Pavement Engineering*, 11(4), 2010.

28. Losa, M., Leandri, P., and Bacci, R. "Measurements of Pavement Macrotexture with Stationary and Mobile Profilometers." *Fifth International Conference on Maintenance and Rehabilitation of Pavements and Technological Control*, Park City, UT, 2007.

29. Losa, M., Leandri, P., and Bacci, R. "Rolling Noise Prediction Models Based on Pavement Surface Characteristics," *Road Materials and Pavement Design,* 2005.

30. Masad, E., Rezaei, A., Chowdhury, A. & Harris, P., 2009. *PREDICTING ASPHALT MIXTURE SKID RESISTANCE BASED ON AGGREGATE CHARACTERISTICS,* College Station, Texas: TEXAS TRANSPORTATION INSTITUTE.

31. Masad, E., Rezaei, A., Chowdhury, A., and Freeman, T. "Field Evaluation of Asphalt Mixture Skid Resistance and Its Relationship to Aggregate Characteristics." *Texas Transportation Institute*, Report No. FHWA/TX-10/0-5627-2, Austin, Texas, 2010.

32. Masad, E., Rezaei, A., Chowdhury, A., and Harris, P. "Predicting Asphalt Mixture Skid Resistance Based on Aggregate Characteristics." *Texas Transportation Institute*, Report No. FHWA/TX-09/0-5627-1, 2009.

33. Meyer, W. E. "Synthesis of Frictional Requirements Research." *Federal Highway Administration (FHWA),* Report No. FHWA/RD-81/159, Washington, DC, 1982.

34. Micro-Epsilon. "OptoNCDT 1700 Instruction Manual." 2010.

35. Miller, T. et al., 2012. Characterization of Asphalt Pavement Surface Texture. *Transportation Research Record: Journal of the Transportation Research Board.*

36. National Cooperative Highway Research Program. "Evaluation of Pavement Friction Characteristics: A Synthesis of Highway Practice." National Cooperative Highway Research Program, Synthesis Report 291, Washington, DC, 2000.

37. Noyce, D. Bahia, H., Yambo, J., Chapman, J., and Bill, A. "Incorporating Road Safety into Pavement Management: Maximizing Surface Friction for Road Safety Improvements." *Midwest Regional University Transportation Center*, Project 04-04, University of Wisconsin – Madison, 2007.

38. PIARC, 1995. International PIARC Experiment to Compare and Harmonize Texture and Skid Resistance Measurements, Brussels, Belgium: Permanent International Association of Road Congresses.

39. Rado, Z. "Vehicle/Pavement Surface Interaction and Impact of Skid on Crash Rates." *59th Annual Ohio Transportation Engineering Conference*, 2005.

40. Rojas, R., 1996. Neural Networks: A Systematic Introduction. Germany: Springer.

41. Sakhaeifar, M. S., Sh.Underwood, B. & Kim, Y. R., 2010. Development of Artificial Neural Network Predictive Models for Populating Dynamic Moduli of Long-Term Pavement Performance Sections. *Transportation Research Record: Journal of the Transportation Research Board,* Volume 2181, p. 88–97.

42. Sandberg, U. and Ejsmont, J. "Noise Emission, Friction and Rolling Resistance of Car Tires: Summary of an Experimental Study." *National Conference on Noise Control Engineering*, Newport Beach, California, 2000.

43. Wessex Test Equipment. "Wessex Skid Tester S885 Operating Instructions." 2008.

44. Zofka, A. & Yut, I., 2012. Prediction of Asphalt Creep Compliance using Artificial Neural Networks, s.l.: Archives of Civil Engineering.

APPENDIX A: SLP ANALYSIS METHOD TEMPLATES

▲	A	B	C	D	E	F	G	H	I	J	K	L	M	N
1	▙▗▟▙▖▙▟▙		▙▟▗▙▞▙▙		▙▙▙▟▙▙▙		▙▙▙▙▙		▙▟▙▙		▙▙▙▟▙▙		▙▙▙▙▙	
2	prof1_rep1		prof2_rep1		prof3_rep1		prof4_rep1		prof5_rep1		prof1_rep2		prof2_rep2	
3	8.9995	0	8.9721	65012	9.0076	70	8.9359	69	9.0525	69	8.9303	71	8.9802	67
4	8.9914	29	8.9721	65011	9.0232	69	9.0051	68	9.0051	68	8.9484	70	9.0082	66
5	8.9852	28	8.9478	65010	9.0014	68	10.1012	67	8.9633	67	8.9446	69	9.0001	65
6	8.939	27	8.9471	65009	9.0026	67	10.1012	66	8.9995	66	8.9185	68	9.0051	64
7	8.9291	26	8.9397	65008	9.0219	66	9.4862	65	8.9989	65	8.9241	67	9.0045	63
8	8.9297	25	8.9397	65007	9.0475	65	9.4899	64	8.997	64	8.9353	66	8.9933	62
9	8.9328	24	8.9615	65006	9.0593	64	9.4937	63	8.9951	63	8.9341	65	8.9989	61
10	8.9422	23	8.9683	65005	9.0543	63	9.4924	62	8.9864	62	8.9266	64	9.0051	60
11	8.9565	22	8.9615	65004	9.0562	62	10.1012	61	8.9957	61	8.9228	63	9.0026	59
12	8.9459	21	8.9552	65003	9.0369	61	8.9235	60	9.012	60	8.926	62	8.9951	58
13	8.9503	20	8.9471	65002	9.0244	60	8.9322	59	8.9926	59	8.9203	61	8.9764	57
14	8.9559	19	8.9471	65001	9.0282	59	8.9434	58	8.9789	58	8.9197	60	8.9403	56
15	8.9584	18	8.9471	65000	9.0412	58	8.9284	57	8.9789	57	8.9135	59	8.9453	55
16	8.9446	17	8.9615	64999	9.0543	57	8.9191	56	9.002	56	8.9154	58	8.9989	54
17	8.9216	16	8.9353	64998	9.0842	56	8.9147	55	9.0007	55	8.9085	57	8.9546	53
18	8.9372	15	8.8992	64997	9.1104	55	8.9216	54	9.0014	54	8.911	56	8.939	52
19	8.9054	14	8.8593	64996	9.1123	54	8.949	53	9.0232	53	8.9098	55	8.8979	51
20	8.926	13	8.8655	64995	9.1011	53	8.9665	52	9.0506	52	8.9303	54	8.9079	50
21	8.9484	12	8.8761	64994	9.1023	52	8.9652	51	9.0456	51	8.9509	53	8.9098	49
22	8.9091	11	10.1012	64993	9.111	51	8.9316	50	9.0462	50	8.9203	52	8.9197	48
23	8.8979	10	10.1012	64992	9.1304	50	8.9048	49	9.0462	49	8.9098	51	8.9328	47
24	8.9066	9	10.1012	64991	9.1079	49	8.8773	48	9.0419	48	8.9154	50	8.9459	46
25	8.9752	8	8.9185	64990	9.0556	48	8.878	47	9.0294	47	8.9197	49	8.9546	45

◄ ◄ ► ►◄ TSA SUMMARY / MPD SUMMARY / **RAW DATA STATION 1** / 4096 COND STAT1 PROF1 rep1 / 4096 DFT STAT1_PROF1

Figure 17. Screenshot. SLP raw data processing template.

	A	B	C	D	E	F	G	H	I	J	K	L	M
1													
2		RAW	TRANSFORMED DATA		INVERSION AND DROPOUTS				RESAMPLED 2:1				
3	i	Raw Z	Corrected Z (mm)	X (mm)	Inverted Z (mm)	Z, No Dropouts (mm)	Z, No Dropouts + Shift (mm)	Dropout Count	Z, No Dropouts (mm)	X (mm)			
4	0	8.9995	36.0	0.0667	24.0	24.00	24.00	0	24.0344	0.133			
5	1	8.9914	36.0	0.1333	24.0	24.03	24.03	0	24.244	0.267		Frequency (Hz)	1250
6	2	8.9852	35.9	0.2000	24.1	24.06	24.06	0	24.2812	0.400		Measuring Speed (m/s)	0.037
7	3	8.939	35.8	0.2667	24.2	24.24	24.24	0	24.2312	0.533		Δx (points/mm)	15
8	4	8.9291	35.7	0.3333	24.3	24.28	24.28	0	24.2164	0.667		Point Count	8192
9	5	8.9297	35.7	0.4000	24.3	24.28	24.28	0	24.1764	0.800		Dropout Count	59
10	6	8.9328	35.7	0.4667	24.3	24.27	24.27	0	24.2216	0.933		Dropout Rate	0.7%
11	7	8.9422	35.8	0.5333	24.2	24.23	24.23	0	24.2512	1.067		Required Points	8192
12	8	8.9565	35.8	0.6000	24.2	24.17	24.17	0	24.296	1.200		Trimmed Points	0
13	9	8.9459	35.8	0.6667	24.2	24.22	24.22	0	24.3636	1.333		Inversion Threshold	60
14	10	8.9503	35.8	0.7333	24.2	24.20	24.20	0	24.3736	1.467		Dropout Threshold	20
15	11	8.9559	35.8	0.8000	24.2	24.18	24.18	0	23.9996	1.600		Shift (mm)	0
16	12	8.9584	35.8	0.8667	24.2	24.17	24.17	0	23.9972	1.733			
17	13	8.9446	35.8	0.9333	24.2	24.22	24.22	0	24.2736	1.867			
18	14	8.9216	35.7	1.0000	24.3	24.31	24.31	0	23.9272	2.000			
19	15	8.9372	35.7	1.0667	24.3	24.25	24.25	0	23.7752	2.133			
20	16	8.9054	35.6	1.1333	24.4	24.38	24.38	0	23.7928	2.267			
21	17	8.926	35.7	1.2000	24.3	24.30	24.30	0	23.8872	2.400			
22	18	8.9484	35.8	1.2667	24.2	24.21	24.21	0	24.2488	2.533			
23	19	8.9091	35.6	1.3333	24.4	24.36	24.36	0	24.2812	2.667			
24	20	8.8979	35.6	1.4000	24.4	24.41	24.41	0	24.2288	2.800			
25	21	8.9066	35.6	1.4667	24.4	24.37	24.37	0	24.2412	2.933			
26	22	8.9752	35.9	1.5333	24.1	24.10	24.10	0	24.234	3.067			
27	23	9.0001	36.0	1.6000	24.0	24.00	24.00	0	24.1692	3.200			
28	24	8.9901	36.0	1.6667	24.0	24.04	24.04	0	24.2116	3.333			
29	25	9.0007	36.0	1.7333	24.0	24.00	24.00	0	24.2264	3.467			
30	26	8.9721	35.9	1.8000	24.1	24.11	24.11	0	24.1816	3.600			

Sheet tabs: TSA SUMMARY | MPD SUMMARY | RAW DATA STATION 1 | **4096 COND STAT1_PROF1_rep1** | 4096 DFT STAT1_PROF1_rep1 | 4096 MPD STAT1_PROF1_rep1 | 4096 CON...

Charts: Inverted Profile; Trimmed Profile

Figure 18. Screenshot. SLP data conditioning template.

44

Use this template for field sections

Analysis Inputs		
baseline (m)	0.546	
N	4096	
Δz (m)	0.000133	
Δf_{xx}	1.831	
1/3 O.B. Max (mm)	36.4	
O.B. Max (mm)	109.2	

Slope, Offset Suppresion Windowing		
b_1	2.3E-07	
b_2	0.02	
Σw_i	0.94	
SCBW low	410	
SCBW high	3686	

Octave Band Texture Parameters (L_{TX})		
λ_n	L_{TX}	a_λ
0.5	38.2	0.08
1	40.7	0.11
2	42.6	0.13
4	44.7	0.17
8	45.9	0.20
16	44.7	0.17
32	39.2	0.09
64	40.0	0.10
128	39.3	0.09

DIAGNOSTICS

Energy Control in Octave Bands
$Z_{PSD,k}\cdot\Delta f_{xx}$		$\Sigma Z_{p,n}$
1.62E-07	Ok	1.62E-07

Energy Control in 1/3 Octave Bands
$Z_{PSD,k}\cdot\Delta f_{xx}$		$\Sigma Z_{p,n}$
1.43E-07	Ok	1.43E-07

Theorem of Parseval
8.79E-04	Ok	8.79E-04

	CONDITIONING INPUT			SLOPE & OFFSET SUPPRESSION		WINDOWING				DISCRETE FOURIER TRANSFORM (DFT)		POWER SPECTRAL DENSITY (PSD)			NARROW BANDS		
i	z (m)	$z_{i,1,1}$ (mm)	z_i (m)	b_i	Z_i	w_i	w^2_i	$Z_{i,win}$	$Z^2_{i,win}$	Z_k	$|Z_k|^2$	$Z_{PSD,k}$	L_{txk}	$Z_{PSD,k}\cdot\Delta f$	$f_{xx,low}$	f_{xx}	$f_{xx,up}$
0	0.00013	24.0344	0.0240	-8.6E-09	-2.2E-04	0.00	0.00	-8.8E-37	7.8E-73	9.9386961420	5.9E-10	6.4E-10	30.7	1.2E-09	0.0	0.9	1.8
1	0.00027	24.244	0.0242	-8.7E-09	-1.1E-05	0.00	0.00	-1.7E-10	3.0E-20	-0.5761211125	2.0E-08	2.2E-08	46.0	4.0E-08	1.8	2.7	3.7
2	0.00040	24.2812	0.0243	-8.7E-09	2.6E-05	0.00	0.00	1.6E-09	2.7E-18	0.276323643	5.1E-09	5.6E-09	40.1	1.0E-08	3.7	4.6	5.5
3	0.00053	24.2312	0.0242	-8.7E-09	-2.4E-05	0.00	0.00	-3.4E-09	1.2E-17	0.126374827	1.2E-09	1.3E-09	33.8	2.4E-09	5.49	6.4	7.3
4	0.00067	24.2164	0.0242	-8.6E-09	-3.9E-05	0.00	0.00	-9.9E-09	9.8E-17	0.146294683	1.3E-09	1.4E-09	34.1	2.6E-09	7.3	8.2	9.2
5	0.00080	24.1764	0.0242	-8.6E-09	-7.9E-05	0.00	0.00	-3.1E-08	9.8E-16	-0.125920706	1.8E-09	2.0E-09	35.6	3.6E-09	9.2	10.1	10.99
6	0.00093	24.2216	0.0242	-8.6E-09	-3.5E-05	0.00	0.00	-2.0E-08	3.8E-16	5.1933420248	5.6E-10	6.1E-10	30.5	1.1E-09	11.0	11.9	12.8
7	0.00107	24.2512	0.0243	-8.6E-09	-5.2E-06	0.00	0.00	-4.0E-08	1.6E-17	-0.1147858830	1.4E-09	1.6E-09	34.6	2.9E-09	12.8	13.7	14.6
8	0.00120	24.296	0.0243	-8.7E-09	3.9E-05	0.00	0.00	4.0E-08	1.6E-15	6.8243125247	4.4E-10	4.8E-10	29.4	8.8E-10	14.6	15.6	16.5
9	0.00133	24.3636	0.0244	-8.7E-09	1.1E-04	0.00	0.00	1.4E-07	1.8E-14	0.1400030469	1.6E-09	1.8E-09	35.1	3.2E-09	16.5	17.4	18.3
10	0.00147	24.3736	0.0244	-8.7E-09	1.2E-04	0.00	0.00	1.8E-07	3.4E-14	5.9148646919	2.6E-10	2.9E-10	27.2	5.2E-10	18.3	19.2	20.1
11	0.00160	23.9996	0.0240	-8.5E-09	-2.6E-04	0.00	0.00	-4.9E-07	2.4E-13	-5.1480496102	7.4E-10	8.1E-10	31.7	1.5E-09	20.1	21.1	22.0
12	0.00173	23.9972	0.0240	-8.5E-09	-2.6E-04	0.00	0.00	-5.9E-07	3.5E-13	-6.2445261403	2.5E-10	2.7E-10	27.0	5.0E-10	22.0	22.9	23.8
13	0.00187	24.2736	0.0243	-8.6E-09	1.6E-05	0.00	0.00	4.2E-08	1.8E-15	4.0419378042	4.3E-10	4.7E-10	29.3	8.5E-10	23.8	24.7	25.6
14	0.00200	23.9272	0.0239	-8.5E-09	-3.3E-04	0.00	0.00	-1.0E-06	1.0E-12	7.8362286979	6.9E-10	7.5E-10	31.4	1.4E-09	25.6	26.6	27.5
15	0.00213	23.7752	0.0238	-8.4E-09	-4.8E-04	0.00	0.00	-1.7E-06	2.9E-12	-4.426003025	5.3E-10	5.8E-10	30.3	1.1E-09	27.5	28.4	29.3
16	0.00227	23.7928	0.0238	-8.4E-09	-4.7E-04	0.00	0.00	-1.9E-06	3.5E-12	-5.785309950	2.1E-10	2.3E-10	26.2	4.1E-10	29.3	30.2	31.1
17	0.00240	23.8872	0.0239	-8.5E-09	-3.7E-04	0.00	0.00	-1.7E-06	2.8E-12	5.0674752057	6.6E-10	7.2E-10	31.2	1.3E-09	31.1	32.0	33.0
18	0.00253	24.2488	0.0242	-8.6E-09	-1.0E-05	0.00	0.00	-5.1E-08	2.6E-15	1.8558148017	2.1E-11	2.3E-11	16.2	4.1E-11	33.0	33.9	34.8
19	0.00267	24.2812	0.0243	-8.6E-09	2.2E-05	0.01	0.00	1.3E-07	1.6E-14	-0.1236363856	9.2E-10	1.0E-09	32.6	1.8E-09	34.8	35.7	36.6
20	0.00280	24.2288	0.0242	-8.6E-09	-3.1E-05	0.01	0.00	-1.9E-07	3.7E-14	-1.2108486073	6.7E-11	7.3E-11	21.2	1.3E-10	36.6	37.5	38.5
21	0.00293	24.2412	0.0242	-8.6E-09	-1.8E-05	0.01	0.00	-1.3E-07	1.6E-14	3.5546267315	8.4E-11	9.1E-11	22.2	1.7E-10	38.5	39.4	40.3
22	0.00307	24.234	0.0242	-8.6E-09	-2.6E-05	0.01	0.00	-2.0E-07	3.8E-14	-1.0410444114	7.0E-12	7.6E-12	11.5	1.4E-11	40.3	41.2	42.1
23	0.00320	24.1692	0.0242	-8.5E-09	-9.1E-05	0.01	0.00	-7.5E-07	5.7E-13	4.7314105689	1.6E-10	1.7E-10	25.0	3.2E-10	42.1	43.0	43.9
24	0.00333	24.2116	0.0242	-8.6E-09	-4.9E-05	0.01	0.00	-4.4E-07	1.9E-13	5.945048547	9.6E-10	1.0E-09	32.8	1.9E-09	43.9	44.9	45.8
25	0.00347	24.2264	0.0242	-8.6E-09	-3.4E-05	0.01	0.00	-3.3E-07	1.1E-13	3.4382530680	1.2E-10	1.3E-10	23.9	2.5E-10	45.8	46.7	47.6
26	0.00360	24.1816	0.0242	-8.5E-09	-7.9E-05	0.01	0.00	-8.4E-07	7.0E-13	-9.878589302	6.2E-10	6.7E-10	30.9	1.4E-09	47.6	48.5	49.4
27	0.00373	24.1516	0.0242	-8.5E-09	-1.1E-04	0.01	0.00	-1.2E-06	1.6E-12	-1.5076675499	1.7E-09	1.8E-09	35.2	3.3E-09	49.4	50.4	51.3
28	0.00387	24.0396	0.0240	-8.5E-09	-2.2E-04	0.01	0.00	-2.7E-06	7.4E-12	1.7241767792	4.8E-10	5.2E-10	29.8	9.5E-10	51.3	52.2	53.1
29	0.00400	24.2264	0.0242	-8.5E-09	-3.5E-05	0.01	0.00	-4.6E-07	2.1E-13	7.5602286488	3.5E-10	3.8E-10	28.4	6.9E-10	53.1	54.0	54.9
30	0.00413	24.2016	0.0242	-8.5E-09	-6.0E-05	0.01	0.00	-8.5E-07	7.2E-13	2.2088799105	3.0E-11	3.2E-11	17.7	5.9E-11	54.9	55.8	56.8
31	0.00427	24.1916	0.0242	-8.5E-09	-7.0E-05	0.01	0.00	-1.1E-06	1.1E-12	-1.0847897585	5.2E-10	5.7E-10	30.2	1.0E-09	56.8	57.7	58.6
32	0.00440	24.2864	0.0243	-8.5E-09	2.4E-05	0.01	0.00	3.9E-07	1.5E-13	-0.1521908292	2.0E-09	2.2E-09	36.1	4.1E-09	58.6	59.5	60.4

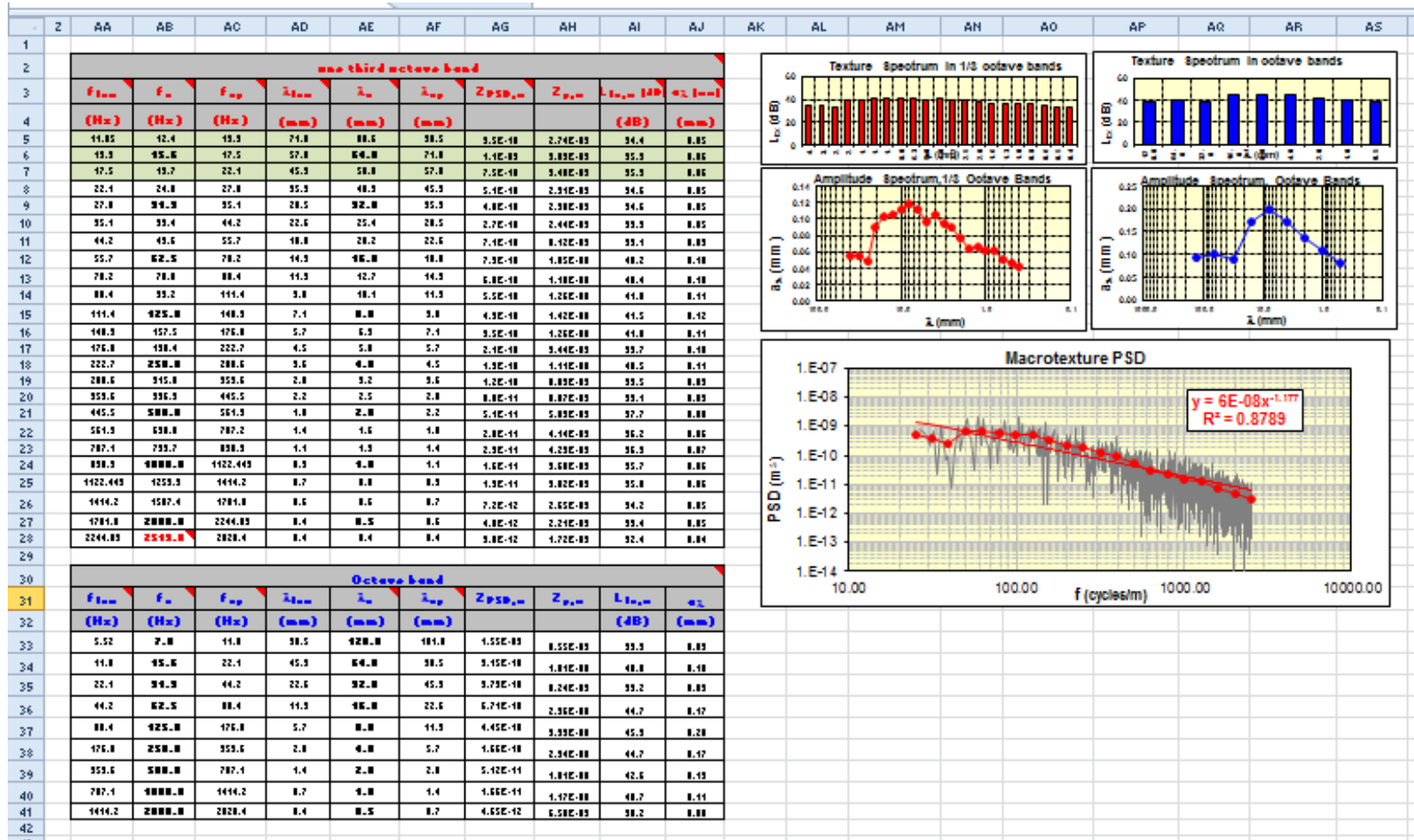**Figure 19. Screenshot. SLP data analysis template inputs.**

Figure 20. Screenshot. SLP data analysis template outputs.

46

	A	B	C	D	E	F	G	H	I	J	K
1	ISO 13473-1 Alternative 2					ISO 13473-1 Alternative 1					
2	Δx (mm)	Amplitude (mm)	Low Pass Filter @ λ=20 mm	High Pass Filter @ λ=50 mm	Low Pass Filter @ λ=2.5 mm	Amplitude (mm)	Low Pass Filter @ λ=2.5 mm	Slope Supression (Regression)			
3	0.000		24.00	-24.00	-24.15		-24.15			Mean Profile Depth Calculation (mm)	
4	0.067		24.02	-24.02	-24.16		-24.16			First Half of Segment (A)	
5	0.133		24.03	-24.03	-24.16		-24.16			Baseline Length	100 mm
6	0.200		24.08	-24.08	-24.16		-24.16			Alternative 1	0.33
7	0.267		24.12	-24.12	-24.17		-24.17			Alternative 2	0.33
8	0.333		24.15	-24.15	-24.17		-24.17			Second Half of Segment (B)	
9	0.400		24.17	-24.17	-24.17		-24.17			Baseline Length	100 mm
10	0.467		24.18	-24.18	-24.17		-24.17			Alternative 1	0.34
11	0.533		24.18	-24.18	-24.17		-24.17			Alternative 2	0.33
12	0.600		24.18	-24.18	-24.17		-24.17				
13	0.667		24.18	-24.18	-24.17		-24.17			Average MPD Value	
14	0.733		24.18	-24.18	-24.17		-24.17			Alt 1 (ISO 13473-1)	0.33
15	0.800		24.18	-24.18	-24.17		-24.17			Alt 2 (ISO 13473-1)	0.33
16	0.867		24.18	-24.18	-24.17		-24.17				
17	0.933		24.19	-24.19	-24.17		-24.17				
18	1.000		24.20	-24.20	-24.17		-24.17				
19	1.067		24.21	-24.21	-24.17		-24.17				
20	1.133		24.21	-24.21	-24.17		-24.17				
21	1.200		24.21	-24.21	-24.17		-24.17				
22	1.267		24.22	-24.22	-24.17		-24.17				
23	1.333		24.23	-24.23	-24.17		-24.17				
24	1.400		24.23	-24.23	-24.17		-24.17				
25	1.467		24.23	-24.23	-24.18		-24.18				
26	1.533		24.22	-24.22	-24.18		-24.18				
27	1.600		24.21	-24.21	-24.18		-24.18				
28	1.667		24.20	-24.20	-24.18		-24.18				
29	1.733		24.20	-24.20	-24.18		-24.18				
30	1.800		24.20	-24.20	-24.18		-24.18				
31	1.867		24.20	-24.20	-24.18		-24.18				
32	1.933		24.20	-24.20	-24.18		-24.18				
33	2.000		24.18	-24.18	-24.18		-24.18				
34	2.067		24.17	-24.17	-24.18		-24.18				
35	2.133		24.16	-24.16	-24.18		-24.18				

Figure 21. Screenshot. MPD data analysis template.

University of Wisconsin-Madison

Department of Civil and Environmental Engineering

1410 Engineering Drive, Room 270

Madison, WI 53706

Phone: 608-263-3175

Fax: 608-263-2512

cfire.wistrans.org